Check for updates

ChemCatChem

Review
doi.org/10.1002/cctc.202301560

Chemistry Europe
European Chemical Societies Publishing

www.chemcatchem.org

Hot Paper

Nitrogen-Based Imperfections in Graphitic Carbon Nitride – New Trend for Enhancing Photocatalytic Activity?

Zafer Eroglu,[a] Melek Sermin Ozer,*[a] and Önder Metin*[a]

In honor of the 100th anniversary of the Republic of Türkiye, this paper is dedicated to the resilient spirit, visionary leadership, and enduring legacy of those who contributed to the foundation and development of the Republic of Türkiye.

This review comprehensively explores the engineering of nitrogen vacancies (N-vacancies) in polymeric carbon nitride (CN) and uncovering their profound impact on the photocatalytic applications of CN. The intentional creation of N-vacancies in CN obtained by removing the targeted N atoms emerges as a crucial strategy for fine-tuning its photo(catalytic)physical properties. Defect-centric investigations illuminate enlarged surface areas, increased substrate interactions and spotlight the correlation between N-vacancy and photoredox transformations. Key N-vacancies (NH_x, N_{2C}, N_{3C}) play exceptional roles in elevating the photocatalytic activity of CN. Besides comprehensively navigating the competitive literature of CN research, this review highlights the controlled manipulation of N-vacancies in CN as an instrumental avenue for customized property tailoring. Additionally, it provides a perspective on the generation of N-vacancies considering temperature, time, and reaction atmosphere by inspecting available synthesis strategies, particularly thermal treatments, along with advanced characterization techniques shedding light on the profound influence of N-vacancies on the structural and electronic properties of CN. Moreover, this review underlines the impact of defects in CN on its photocatalytic performance, tuning bandgaps, midgap state formation, and creating active sites within the lattice. The versatile strategy employed in vacancy engineering within CN shows great potential for designing new-generation photocatalysts with tailored functionalities.

1. Introduction

Carbon nitride (CN), despite having a history spanning two centuries, has gained significant scientific inspiration following the groundbreaking discovery of graphene in recent years, propelling the utilization of carbon-based two-dimensional (2D) nanomaterials across various scientific disciplines.[1,2] Through years of extensive research activities, CN emerged as a N-rich carbon-based material with a distinct 3:4 (C:N) ratio, exhibiting distinguished properties, notably functioning as a 2D semiconductor photocatalyst.[2,3] Polymeric CN possesses sp^2-hybridized carbon and N atoms, forming tri-s-triazine units interconnected via sp^3-hybridized NH-binding linkers (Figure 1a). These layers are connected by weak van der Waals forces, resulting in a graphite-like structure. The attention to both structural and physical aspects has been a focal point for scholars in this domain.[2] Prof. Markus Antonietti's pioneering work on the photocatalytic production of hydrogen catalyzed substantial exploration into CN's electronic properties.[4] After that, the usage of polymeric CN has surpassed traditional metal oxide photocatalysts like TiO_2 and ZnO, primarily due to its superior photophysical and chemical features.[5] CN stands out as a non-metallic semiconductor with a bandgap of 2.7 eV (454 nm), displaying excellent visible light absorption capabilities. Its valence band (VB) and conduction band (CB) potentials, reported as approximately +1.4 V and −1.3 V respectively, make it as a good photocatalysts for various photoredox reactions, spanning from water splitting to organic transformations.[2,5] Despite its remarkable attributes, CN has faced several challenges in its photocatalytic applications due to the issues regarding poor charge separation, low surface area and rapid recombination.[5–10] To overcome these issues, researchers have explored proper ways for the structural manipulation of CN, exploiting its C and N constituents. Moreover, its highly functionalized nature allows for diverse modification approaches.[5,11] Various precursors such as urea, melamine, and dicyanamide have been explored for the synthesis of CN via the high-temperature polycondensation method (Figure 1b).[12] These precursors along with other compatible small molecules offer avenues for band engineering, which enhances the photocatalytic activity of CN.[13] With the purpose of boosting the limited responsiveness of CN to longer wavelengths and quick depletion of charge carriers, various common techniques including metal/nonmetal elemental doping, defect decoration, heterojunction formation, covalent/non-covalent functionalization and etc. are utilized to control the composition, electronic properties, redox potential, movement of charge carriers, and active sites.[9,14–18] Among them, defect engineering viewed as imperfections in materials leading to random alterations in lattice positions, which result in the

[a] Dr. Z. Eroglu, Dr. M. S. Ozer, Prof. Ö. Metin
Department of Chemistry, College of Sciences, Koç University, 34450 Sarıyer, Istanbul, Türkiye
E-mail: melekozer@ku.edu.tr
ometin@ku.edu.tr

© 2024 The Authors. ChemCatChem published by Wiley-VCH GmbH. This is an open access article under the terms of the Creative Commons Attribution Non-Commercial License, which permits use, distribution and reproduction in any medium, provided the original work is properly cited and is not used for commercial purposes.

© 2024 The Authors. ChemCatChem published by Wiley-VCH GmbH

creation of empty spaces has been studied intensively.[6,19–22] Rearranging the order of atoms in the crystalline structure using this approach considered to enhancing the efficiency of photogenerated charge carriers by creating midgap states.[23,24] These newly formed states lay between the CB and VB of the corresponding material, and thus delaying the recombination of photogenerated holes and electrons. However, such defects are also reported to create disadvantages such as low selectivity due to the emerged excess vacancies might lead to a side reaction.[25] In addition to the changes observed in photophysical properties, the morphological and surface properties are also improved compared to that of pristine CN. The vacancies of C and N atoms in a CN structure result in the increased porosity and a larger surface area, contributing to a higher number of active sites.[26,27]

The effectiveness of incorporating vacancies in CN structures depends on the specific application and the desired material properties. These vacancies provide additional reaction sites, promoting the photocatalytic reactions and making them highly effective processes such as pollutant degradation[28,29] and hydrogen evolution[30] reactions. Similarly, in fields like electronics and photovoltaics, the increased electron mobility resulting from vacancies can improve the activity of the material, making it useful for various electronic devices.[31] Furthermore, in optoelectronic applications, the altered optical properties due to these vacancies can improve the proficiency of devices like sensors, photodetectors, and solar cells.[32–35] However, it is essential to note that not all applications benefit equally from vacancies created in CN structures. In some cases, such as certain types of sensors or specific (photo)catalytic reactions, the presence of vacancies might introduce undesired side reactions or alter the material's stability, making it less effective.[36] Moreover, the effectiveness of vacancies can also depend on the concentration and distribution of these defects within the material. Therefore, careful consideration of the specific application requirements and systematic experimental testing are necessary to determine whether incorporating vacancies is advantageous or not.[37–39]

Certainly, the controlled manipulation of atomic vacancies within the CN structure is pivotal in tailoring its properties for specific applications. Achieving the desired material characteristics necessitates a careful approach wherein the removal of C or N atoms from the lattice is precisely depending upon the target application. It is not merely the elimination of these atoms that is significant; the regulation of vacancy content and the strategic creation of active sites within the lattice hold importance.[21,22,30,37] Understanding the influence of a specific defect demands a comprehensive analysis. In this respect, this review focuses specifically on nitrogen vacancies (N-vacancies) within polymeric CN structure, exploring the details of how these vacancies influence the material's photophysical, chemical and correlation with respect to photocatalytic application. Moreover, advanced characterization techniques are employed to distinguish and quantify these created spaces, enabling a deep comprehension of the structural alterations induced by N-vacancies. Conclusively, this review closes by delineating challenges, providing an insightful outlook, and delving into future aspects, all aimed at catalyzing advancements in the field of N-vacancy CN for various photocatalytic applications. The meticulous examination of challenges, combined with a forward-looking perspective, aspires to contribute to the ongoing progression of knowledge and innovation within the domain.



Onder Metin received his PhD degree in Chemistry from Middle East Technical University in 2010. He studied as a research fellow at Brown University in 2009 and then at Darmstadt Technical University in 2010. He was a postdoctoral research associate at Brown University in 2012-2013. He is now a Professor of Chemistry and PI of Metin Research Group at Koç University. He received numerous national scientific awards given to the outstanding young scientists. He has served as the Secretary General of Federation of Asian Chemical Societies (FACS). His research interests are nanomaterials, nanocatalysis, photocatalysis, hydrogen storage and sustainable organic transformations.



Melek Sermin obtained her Ph.D. from Universität zu Köln in Organic Chemistry under the supervision of Prof. Albrecht Berkessel. She is currently working as a postdoctoral researcher in Metin Research Group and her research interests are photoredox organic transformations, carbon-based semiconducting materials, particularly carbon-based quantum dots.



Zafer Eroğlu received his B.Sc. in Chemistry Education, M.Sc. and then his Ph.D. in Nanoscience and Nanoengineering from Atatürk University. He holds a position as a postdoctoral researcher in Metin Research Group at Koç University. His research interests are quantum dots, 2D nanomaterials, band engineering, photocatalysis, energy storage, removal of pollutants from wastewater and nanoparticles.

© 2024 The Authors. ChemCatChem published by Wiley-VCH GmbH

18673899, 0, Downloaded from https://chemistry-europe.onlinelibrary.wiley.com/doi/10.1002/cctc.202301560 by Koc University, Wiley Online Library on [12/07/2024]. See the Terms and Conditions (https://onlinelibrary.wiley.com/terms-and-conditions) on Wiley Online Library for rules of use; OA articles are governed by the applicable Creative Commons License

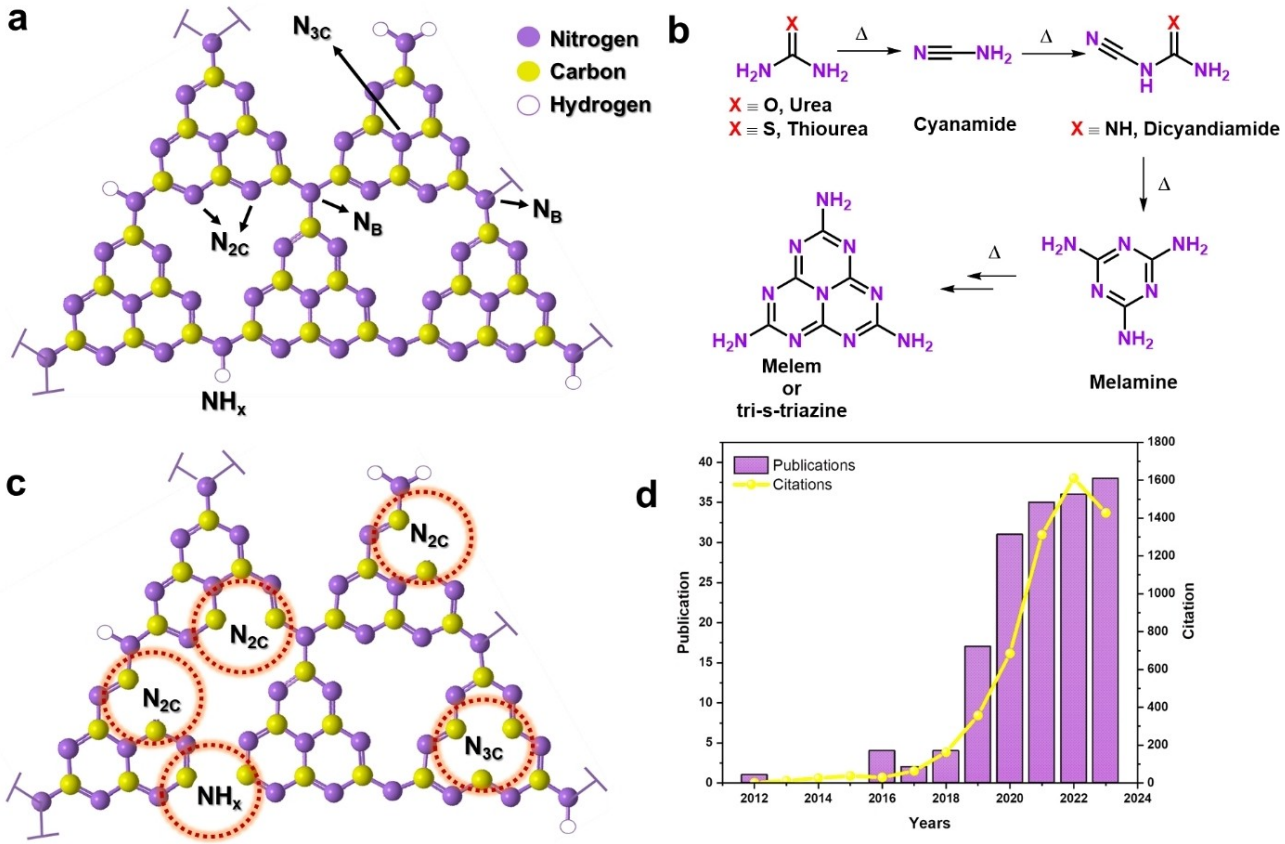


Figure 1. Schematic depiction of **(a)** CN structure, **(b)** the synthesis for CN through thermal polymerization involving various precursors, including urea, thiourea, cyanamide, dicyanamide, and melamine, **(c)** N-vacancy CN structure, **(d)** Publications in journals and citations related to the topics of "carbon nitride" and "N-vacancy" and from 2012 onward according to Web of Science.

2. The effect of N-vacancy-CN on the Photocatalytic Activity

The defects in semiconducting materials make possible to control a photocatalytic activity as needed. The imperfections in semiconducting materials at the atomic/molecular level can exhibit varying degrees of photophysical characteristics. Since the impact of defects on improving the efficiency of a photocatalyst has been proven to be an effective strategy of scientific discussion for years, scholars introduced different types of them.[39–43] Among them, N-vacancy can be classified under the title of point defects, also known as atomic/zero-dimensional defects, where N atoms are less than the accepted scaffold of CN (Figure 1c).[6] The depletion of N atoms in the CN structure can lead to the emergence of additional functional groups, which serve as active sites. These sites, indirectly acting as trapping centers, play a crucial role in enhancing the performance of photogenerated charge carriers where this phenomenon significantly contributes to the improvement of photocatalytic performance.[19] Besides, the symmetrical change in the π-π interactions may affect the delocalization of electrons on the surface and create polarization, which was proved by the theoretical studies. The theoretical calculations revealed that there is higher electron density around the defected area, revealing that they serve as an electron trap region.[44,45] Bandgap tunability is another possibility that may arise from manipulation of reaction parameters during the synthesis of N-vacancy CN. Preserving similar electronic properties, such as bandgap, remains advantageous since defect engineering introduces midgap states, recombination zones, and quantum confinement effects.[40] Compared to pristine CN, an increase in surface area and adsorption capacity, both of which enhance interactions with the relevant substrates involved in the desired reaction, might be enabled by creating defects in the structure. In addition to the charming properties already reported in pristine CN, the introduction of N-vacancies strengthens its connection with various materials, molecules, and metals, resulting in stronger bonds/interactions.

In recent years, there has been a remarkable surge in the study of N-vacancy CN for various applications, especially in photocatalysis, with a notable increase in related literature, as exemplified in Figure 1d (A graph shows the number of papers published with the keywords of "carbon nitride" and "N-vacancy" versus years in the 2012–2024 range). The exponential growth of research in this area is a testament to the heightened scientific interest, and thus it is contemporary landscape that forms the focal point of our review.

© 2024 The Authors. ChemCatChem published by Wiley-VCH GmbH

18673899, 0, Downloaded from https://chemistry-europe.onlinelibrary.wiley.com/doi/10.1002/cctc.202301560 by Koc University, Wiley Online Library on [12/07/2024]. See the Terms and Conditions (https://onlinelibrary.wiley.com/terms-and-conditions) on Wiley Online Library for rules of use; OA articles are governed by the applicable Creative Commons License

3. Unraveling the N-Vacancy Puzzle: Synthesis Strategies

Considering the main ring in the skeleton of CN, tri-s-triazine units, most of the strategies are based on the distortion of the structure by removing N_{3C}/N_{2C}-site or both (Figure 1c). The efforts have been invested on the synthetic methods with different parameters to create the most efficient N-deficient CN.[22] Pioneer works of the researchers listed in this review[3] paved the way of generating defects while figuring out the structure of CN through C/N ratio during optimizing a well-ordered CN structure. The ongoing debate on the formulating the composition of CN resulted in C_6N_8 while understanding the intermediates through constructing a perfect crystallinity in CN structure. As a summary, thanks to those scientists, we are now aware that starting from cyanamide, CN forms as follows; *i)* melamine based products around 350 °C, *ii)* the rearrangement of melamine leads to tri-s-triazine units, *iii)* these melem molecules linked together to generated polymeric structure through a star shape rather than linear chains in close to 520 °C, *iv)* above 600 °C, a slight instability starts, *v)* finally structural decomposition occurs at 700 °C via the removal of N-containing species in the repeating motifs, melem (Figure 1b). The enhanced photocatalytic activity of oxygen-deficient TiO_2 inspired Niu and co-workers for the investigation of N-vacancies in CN.[46] Since then, the treatment of pristine CN thermally or chemically became a well-known methodology in this domain. Albeit there are many methodologies such as plasma treatment (H_2S, H_2),[47–50] cold plasma,[51] Helium ion irradiation,[52] microwave treatment,[53] ball milling method,[54] we will herein limit our discussion on the thermal treatment strategies due to their abundancy in the available literature. These tactics were investigated with the alteration of temperature, time, reaction atmosphere (gas environment), calcination steps, closed/open reaction systems, additives (carbon source, molten salts, alkali metals, acids/bases etc.).[5]

To facilitate the thermal polycondensation process and to elucidate the reaction intermediates, Dong *et al.* employed a thermogravimetric-differential scanning calorimetry analysis (TG-DSC) during the synthesis of CN from urea.[55] The authors concluded that the formation of polymeric CN is completed at 465 °C and CN starts to decompose beyond this temperature as depicted in Figure 2a. However, Niu and co-workers prepared CN derivatives starting from dicyandiamide at 550 or 600 °C with a 2.3 °C/min ramp rate for 4 h and obtained orange colored product.[46] All characterization results indicated the formation of N-vacancy in CN structure at 600 °C. The authors also reported that the N-vacancies significantly enhanced the photocatalytic activity of CN in both Rhodamine B decomposition and water splitting reactions. Later, Hou *et al.* performed two-step calcination of dicyandiamide sequentially in static air at 550 °C

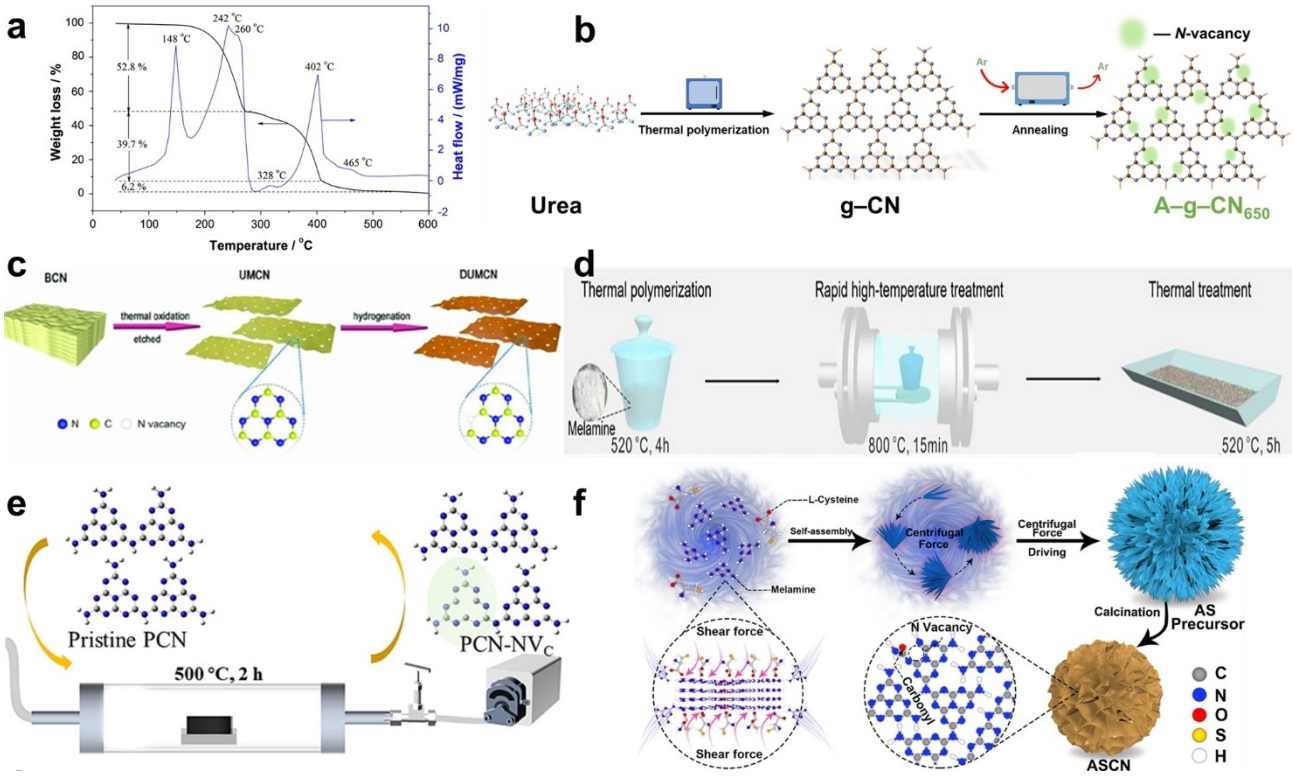


Figure 2. (a) TG-DSC plots during the heating process of urea. Reprinted from.[55] Copyright (2013) with permission from Elsevier. **(b)** Schematic depiction of the synthesis process for N-vacancy CN. Reproduced from.[59] with permission from the Royal Society of Chemistry. **(c)** Graphical representation of the synthesis of DUMCN. Reproduced with permission.[61] Copyright 2020, Wiley. **(d)** Diagram depicting the synthetic pathway for CN-UNS. Reprinted from.[63] Copyright (2022) with permission from Elsevier. **(e)** Procedure for the synthesis of PCN-NVC. Reprinted from.[64] Copyright (2023) with permission from Elsevier. **(f)** Illustration outlining the preparation process of ASCN. Reprinted (adapted) with permission from.[65] Copyright 2023 American Chemical Society.

© 2024 The Authors. ChemCatChem published by Wiley-VCH GmbH

18673899, 0, Downloaded from https://chemistry-europe.onlinelibrary.wiley.com/doi/10.1002/cctc.202301560 by Koc University, Wiley Online Library on [12/07/2024]. See the Terms and Conditions (https://onlinelibrary.wiley.com/terms-and-conditions) on Wiley Online Library for rules of use; OA articles are governed by the applicable Creative Commons License

(4 h with 5 °C/min ramp rate) and then under hydrogen gas flow at 550/600 °C (2 h with 5 °C/min ramp rate).[56] The as-prepared CN-600-H_2 (denoted as N-vacancy CN in this review) showed superior photoelectrocatalytic degradation of 4-chlorophenol owing to enhanced photogenerated charge carriers and surface area after the introduction of deficiencies. In another study, post-calcination at 650 °C under nitrogen atmosphere of urea-based CN for 2 h was prepared and the resultant N-deficient CN was found to have larger surface area and high hydrogen evolution rate.[57] Hu and co-workers introduced N-vacancy in CN through the calcination of melamine at 600, 640, 660, 680 and 700 °C and the latter one demonstrated superior activity in photocatalytic H_2 generation.[58] In a recent study, our research group recently designed an annealing strategy for N-vacancy CN based on TGA results and calcinated urea-based CN at 610, 630 and 650 °C (Figure 2b).[59] This study was unique as it incorporated photoredox organic transformation (oxidative-Mannich reaction) for the first time. The CN prepared at 650 °C exhibited the highest photocatalytic activity and its performance was attributed to the creation of midgap states and various features. A comparable investigation by Dai *et al.* focused on the photocatalytic reduction of nitrobenzene derivatives revealing that pristine CN exhibited superior activity compared to that post-calcinated at 630 °C.[25] On the other hand, to enhance the broad photodetection capabilities of CN, Ghosh *et al.* synthesized a CN starting from urea at 550 °C for 4 h in static air, named N-vacancy CN.[60] Despite no significant change in its photocatalytic activity observed according to the photoluminescence (PL) results, they subsequently subjected this N-deficient CN to further calcination under hydrogen gas at 530 °C for 4 h, achieving the desired activity. Another calcination procedure under hydrogen gas atmosphere at various temperatures was reported by Yang *et al.* as shown in Figure 2c.[61] This procedure exhibited high activity in both hydrogen production and overall water splitting, attributed to the increased presence of active sites in N-vacancy CN. Different approach with the purpose of creating N-vacancy was employed by Zhang *et al.* via multistep calcination of dicyandiamide.[62] They initially elevated the temperature directly to 650 °C for 4 h under an argon gas atmosphere, followed by sequential annealing of the resulting powder at 550 °C for 1 h and finally at 500 °C for 2 h. This unconventional synthesis approach yielded atomic-layered CN with N depletion, enhancing the photocatalytic activity for hydrogen gas evolution under visible light irradiation.

With the motivation of boosted photocatalytic activity of N-vacancy CN, many strategies have been developed such as rapid high temperature treatment and thermal vacuum technologies. As illustrated in Figure 2d, Zhang *et al.* devised a novel technique for the removal of N atoms from the CN skeleton.[63] They subjected pristine CN (derived from melamine) to a temperature range from 20 to 800 °C with an ultrafast heating rate of 600 °C/min, maintaining this temperature for 15 min. Subsequently, the resulting red powder was reheated to 520 °C for 5 h with a slow heating rate of 5 °C/min, yielding excellent results in the hydrogen evolution reaction. In the alternative methodology, melamine-derived CN underwent heating at different temperatures (400, 500, and 600 °C) under vacuum conditions, distinct from other strategies involving alterations to the gas environment (Figure 2e).[64] The thermal vacuum treated CN was specifically employed as photocatalysts for the H_2O_2 production, and the N-deficient CN derivative annealed at 500 °C, exhibited the most favorable photooxidation performance.

Applying additives through the hydro/solvothermal method effectively addresses the previously mentioned limitations of CN in photocatalysis by inducing the formation of N-defects within the structure. An illustrative instance is provided by Kong *et al.*, who employed HNO_3 in conjunction with melamine-based CN at 120 °C for 12 h.[66] The resulting N_{2C} vacancy significantly amplified the photocatalytic performance, demonstrating a enhancement from 4.92 to 30.79 ppm.min^{-1} to in the oxidation of isopropanol to acetone compared to pristine CN. Ammonium persulfate ($(NH_4)_2S_2O_8$) is also used as an additive to create vacancies in CN structure. For example, melamine and $(NH_4)_2S_2O_8$ were blended and subjected to a 12-hour reaction at 120 °C,[67] while in another, a combination involved melamine-based CN at 160 °C for 5 h.[68] The latter approach induced a deficiency in bridging N atoms within the structure, leading to an increase in the photocatalytic applications. Meanwhile, the former method claimed sulfur doping, coupled with the introduction of N_{3C}-vacancies, resulting in the highly efficient production of H_2O_2. In a different instance, melamine-based CN was combined with L-cysteine and subjected to the hydrothermal treatment at 160 °C for 12 h.[69] The oxygen and sulfur-containing nature of L-cysteine not only induced the formation of N-vacancies but also facilitated the doping of these atoms (O and S atoms from L-cysteine) into the CN structure. In another study, Li *et al.* adopted a distinctive approach compared to others by stirring a mixture of melamine and L-cysteine (in a molar ratio of 3:10) using the hydrothermal method (Figure 2f).[65] Subsequently, they subjected the resulting powder to calcination at 500 °C for 2 h under a nitrogen gas environment and obtained enhanced photocatalytic activity in the oxygen reduction to H_2O_2 coupled with 4-methoxybenzyl alcohol oxidation to anisaldehyde. The use of varied carbon sources alongside traditional CN precursors was predominantly applied in synthesis procedures to induce N-defects in the CN structure. For example, both hydrothermal methods, one involving oxalyl dihydrazide-melamine based CN[70] with an ammonia solution at 160 °C for 4 h, and the other utilizing a mixture of peanut oil and dicyandiamide for CN[71] preparation then calcination, led to the formation of N_{2C}-type vacancies in the CN skeleton for photocatalytic hydrogen evolution reaction.

4. Unlocking N-vacancies in CN: Characterization Techniques

The unresolved structural aspects concerning N-vacancy CN persist as a focal point of debate in the scientific community. Researchers are actively engaging in extensive investigations to attain a comprehensive understanding of these difficulties. In

© 2024 The Authors. ChemCatChem published by Wiley-VCH GmbH

18673899, 0, Downloaded from https://chemistry-europe.onlinelibrary.wiley.com/doi/10.1002/cctc.202301560 by Koc University, Wiley Online Library on [12/07/2024]. See the Terms and Conditions (https://onlinelibrary.wiley.com/terms-and-conditions) on Wiley Online Library for rules of use; OA articles are governed by the applicable Creative Commons License

this regard, we will dissect the methodologies that have thus far been employed for the identification of N-vacancies and explore their implications on the material's structural characteristics and catalytic activity. Through a rigorous examination of these techniques, we aim to contribute to the ongoing discourse, providing a nuanced perspective on the structural complexities associated with N-vacancy CN and its consequential impact on functional attributes.

X-ray diffraction (XRD) analysis is a powerful technique used to investigate the crystallographic structure of materials by analyzing the diffraction patterns resulting from X-ray beams interaction. In the case of CN, XRD provides valuable insights into its crystalline nature. The positions and intensities of these peaks are indicative of the arrangement of atoms within the crystal lattice, offering crucial information about the crystallinity, phase composition, and structural characteristics of CN.[72] The powder XRD pattern of a typical CN bears a resemblance to graphite, possessing an intense peak attributed to the interplanar stacking of layers at $2\theta = 27.3^\circ$ (002) and the structural arrangement within the same layer formed by aromatic tri-s-triazine units at $2\theta = 13.1^\circ$ (100).[73,74] The comparison of the former (002) plane in terms of interplanar spacing distance ($d = 0.319$ nm for well-ordered CN) along with its shift in the 2θ angle were encountered after the introduction of N-vacancies.[3] For instance, the calcination of CN in static air at elevated temperatures ($\leq 600\,^\circ C$) was documented to result in a reduction of intensity in both characteristic diffraction peaks in the XRD pattern. Additionally, there was a contraction in interlayer π-π stacking distances from 0.326 to 0.324 nm, accompanied by a slight shift in the (002) plane.[46] Similar results were obtained for the CN synthesized under argon[59,75]/nitrogen[76]/hydrogen gas[77] flow during thermal treatment while air/steam flow[75,78,79] was found to sharpen the (002) peak, indicating the increasing order of CN structure (Figure 3a, b and c). The existence of oxygen gas molecules during synthesis generates polarization on the surface owing to the electronegativity of oxygen atoms, thereby intensifying the interaction between the layers and consequently reducing the interplanar spacing.[75,78,80] Likewise, Shi *et al.* noted a reduction in the distance between CN layers, accompanied by an upward shift in the 2θ angle, with the increased addition of tartaric acid (Figure 3d).[81] Using HNO_3 and H_2O_2 as additives with the purpose of oxidation were also an enhanced prominence of the (100) peak in CN, signifying an increase in plane size and expanded properties.[82] In parallel to this, different methodology with the involvement of HNO_3 and then the calcination under argon gas resulted in a lower angle shift of (002) peak from 27.4° to 26.8°.[83] The addition of molten salts as synthetic strategy was investigated by different groups and the intriguing results were obtained. While Gupta *et al.* found the crystallinity depends on the counter anion of potassium (KX where X is I, Br or Cl) along with a shift toward higher angle,[84] Liu and co-workers used KCl during synthesis and claimed the (100) peak shifted from 13.1 to 8.1 due to K^+ intercalation.[85] The absence of the (100) peak, coupled with the broadening of both peaks, was documented under various conditions, including multi-step calcination,[83,86] treatments involving melamine/$(NH_4)_2S_2O_8$,[67] and the use of KOH[87]/KBH_4,[88] among others.[89]

One of the earliest methods that used to understand structure of polymeric CN and the intermediates during thermal condensation was ***Organic Elemental Analysis (OEA)***. The treatment of various precursors to obtain CN allowed scientist to evaluate the atomic composition and conditions as 600 °C in a sealed quartz ampule led to well-organized polymerization.[3] If the deviation of the value differs from C_6N_8, one can get many information such as incomplete polymerization, defects in CN skeleton, diverse repeating units etc.[2] The reaction balance tilts towards oligomeric and polymeric forms when the open crucible conditions applied. The release of NH_3 and N-containing species further continue under elevated temperatures ($\leq$ 550 °C) and thus leading to cavities in tri-s-triazine motifs.[90] This is evident from increased mass loss and a consequent decrement in the C:N (0.75 for perfect CN) ratio in elemental analysis.[3] Most of the reports discusses the difference in the atomic composition of between the pristine CN and the targeted N-vacancy CN. Sun *et al.* introduced N-vacancies by reducing oxygenated CN under H_2 atmosphere and found that increment in the calcination time provides more N-deficiency in the structure.[80] While a similar finding related to duration of calcination was reported by Liu and co-workers,[91] our group and Zhang *et al.* investigated the effect of temperature and N/C ratio was calculated to be decrease with the elevation of temperature.[59,92]

X-ray Photoelectron Spectroscopy (XPS) is extensively employed to examination of vacancy types in CN and other carbon-based materials. XPS facilitates the analysis of surface elemental composition, providing insights into the interpretation of chemical environments and the identification of removed N types, such as N_{2C}/N_{3C} or N_B. A standard N 1s high resolution spectrum of CN exhibits a prominent signal peak at binding energy of 398.7 eV corresponding to the two-coordinated N atoms (N_{2C}) within the heptazine unit. Additionally, a minor shoulder peak at 400.1 eV is observed, arising from three-coordinated N atoms (N_{3C}) in the same motif. Variations in the polymerization degree are reflected in the N_B signal, which manifests at 401.4 eV.[3] Notably, peaks observed at higher binding energies (402.0–403.0 eV) provide insight into the presence of secondary and primary amines ($-NH_x$) at the molecular edges (Figure 4a).[93] Given the greater prevalence of N_{2C} in comparison to N_{3C}, initial observations of the spectrum may lead to a misinterpretation, as the apparent alteration occurs in the N_{2C} signal region.[46] Therefore, the peak-area ratio of N_{2C}/N_{3C} provides reasonably better evaluation of the lost N atoms in the lattice (Figure 4b). As a consequence of this, the decrease from 3.25 to 0.76 was assumed as the defects mainly located in N_{2C} positions. Moreover, the as-assigned peak of N_{3C} was observed to shift towards higher binding energy, indicating a noteworthy alteration in the electron density surrounding the heptazine rings.[46] Whether employing alkali assistance,[94] subjecting to calcination under nitrogen[95,96]/argon atmosphere,[62] implementing acidic conditions,[66] or utilizing in situ acylation[97] with the intent of inducing defects in CN, similar observations were reported (Figure 4b).

© 2024 The Authors. ChemCatChem published by Wiley-VCH GmbH

18673899, 0, Downloaded from https://chemistry-europe.onlinelibrary.wiley.com/doi/10.1002/cctc.202301560 by Koc University, Wiley Online Library on [12/07/2024]. See the Terms and Conditions (https://onlinelibrary.wiley.com/terms-and-conditions) on Wiley Online Library for rules of use; OA articles are governed by the applicable Creative Commons License

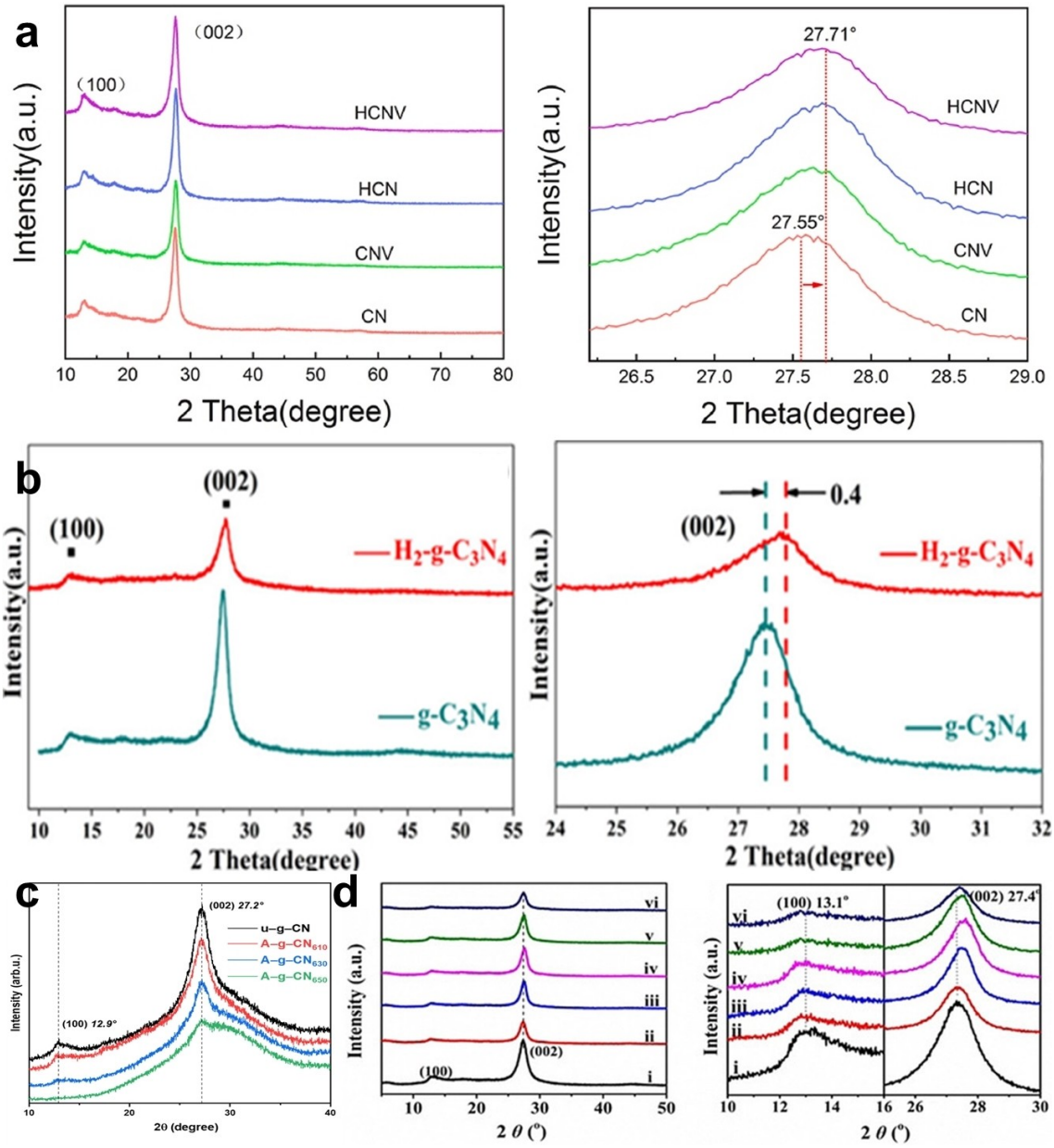


Figure 3. XRD patterns of **(a)** CN, HCN, CNV and HCNV. Reprinted from.[76] Copyright (2023) with permission from Elsevier. **(b)** g-C_3N_4 and H_2-g-C_3N_4. Reprinted (adapted) with permission from.[77] Copyright 2023 American Chemical Society. **(c)** N-vacancy CN. Reproduced from.[59] with permission from the Royal Society of Chemistry. **(d)** DCN and DCN-x. Reproduced with permission.[81] Copyright 2019, Wiley.

In our study and others, the peak ratio of N_{2C} to NH_x was given to understand the location of N-vacancies since the annealing caused the increase in the area of NH_x.[25,59,77,98] This alteration was interpreted as arising from the N_{2C} lattice sites, leading to the loss of delocalization of CN motifs. The change in the chemical environment of C 1s was also discussed and the findings were very crucial about the location of N-defects. In a standard CN, the high resolution C1s spectrum includes N–C–N peak, C-NH_x and adventitious carbon around at 288.0, 286.0 and 284.6 eV, respectively.[59,98] Lin *et al.* synthesized CN from melamine at different temperatures under vacuum and the elimination of N_{3C} resulted in a subtle shift of the predominant peak towards lower binding energy (Figure 4c).[64] Slight changes owing to an augmentation in the electron density surrounding carbon were stated when additional carbon-rich precursors involved in the synthesis methodology (Figure 4d).[99,100] While theoretical calculations indicate that removing NH_x requires less energy compared to N_{2C}, the majority of studies have consistently reported the preferential loss of N_{2C}.[101] Certain reaction conditions, like the previous one,[64] using $CaCO_3$ template,[102] calcination in the presence of air[75] and the use of HNO_3,[83] resulted in the removal of N_{3C} lattice sites. Many strategies alike replacing N atom with an element (P, O and S) or inducing vacancy in the presence of other dopants (Se, Mn, Cu and Mg) contributed to the determination

© 2024 The Authors. ChemCatChem published by Wiley-VCH GmbH

18673899, 0, Downloaded from https://chemistry-europe.onlinelibrary.wiley.com/doi/10.1002/cctc.202301560 by Koc University, Wiley Online Library on [12/07/2024]. See the Terms and Conditions (https://onlinelibrary.wiley.com/terms-and-conditions) on Wiley Online Library for rules of use; OA articles are governed by the applicable Creative Commons License

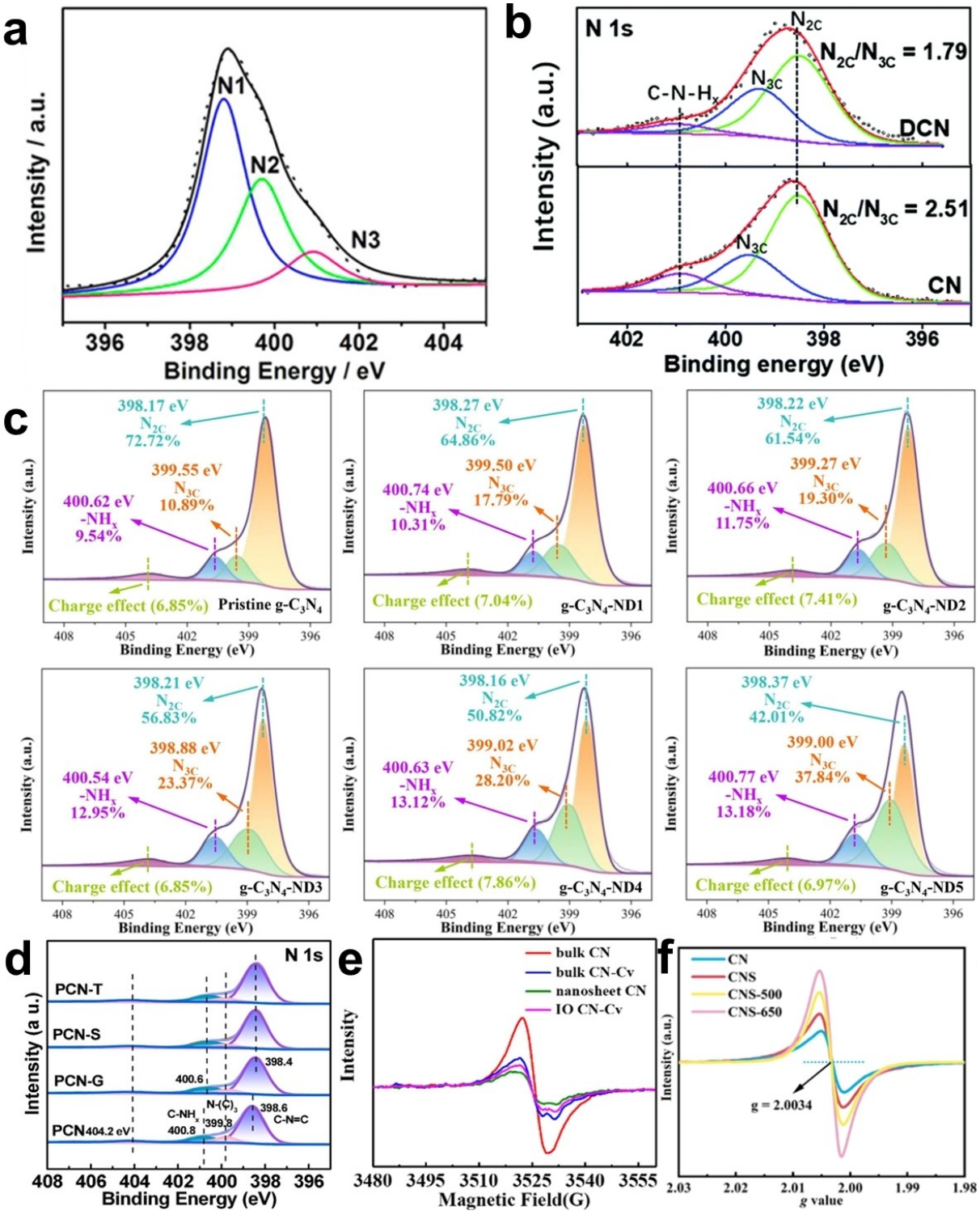


Figure 4. High-resolution XPS spectrum of the N 1s orbital of **(a)** the monolayer mesoporous g-C_3N_4 nanomesh. Reprinted (adapted) with permission from.[93] Copyright 2016 American Chemical Society. **(b)** CN and DCN. Reproduced from[94] with permission from the Royal Society of Chemistry. **(c)** g-C_3N_4, g-C_3N_4-ND1, g-C_3N_4-ND2, g-C_3N_4-ND3, g-C_3N_4-ND4 and g-C_3N_4-ND5. Reprinted from[64] Copyright (2023) with permission from Elsevier. **(d)** PCN, PCN-G, PCN-S and PCN-T. Reprinted from[100] Copyright (2022) with permission from Elsevier. EPR spectra of **(e)** prepared samples. Reprinted (adapted) with permission from.[109] Copyright 2019 American Chemical Society. **(f)** the prepared photocatalysts. Reprinted from[110] Copyright (2022) with permission from Elsevier.

of missing N atom and the location of these atoms by comparing the binding energy changes in XPS.[69,103–108]

All this knowledge to figure out the generated defects in CN in hand, another widely used technique is ***Electron Paramagnetic Resonance (EPR)***, also known as Electron Spin

© 2024 The Authors. ChemCatChem published by Wiley-VCH GmbH

18673899, 0, Downloaded from https://chemistry-europe.onlinelibrary.wiley.com/doi/10.1002/cctc.202301560 by Koc University, Wiley Online Library on [12/07/2024]. See the Terms and Conditions (https://onlinelibrary.wiley.com/terms-and-conditions) on Wiley Online Library for rules of use; OA articles are governed by the applicable Creative Commons License

Resonance (ESR). The fundamental principle of EPR revolves around the interaction of unpaired electron spins with an external magnetic field, causing the absorption or emission of electromagnetic radiation. In the case of CN, EPR serves as a valuable tool for investigating the defects and their quantization within the material. Defects such as N-vacancies and unpaired electrons in the carbon structure exhibit characteristic EPR signals. By subjecting CN samples to an external magnetic field and analyzing the resulting EPR spectra, researchers can gain insights into the nature and concentration of defects present.[43] Since the origin of unpaired electrons are attributed to carbon atoms in CN, the decrease in signal intensity demonstrates the loss of carbon atoms in CN skeleton. Conversely, the observed rise in the peak with a g value (electron spin factor of sample) of two indicates the removal of N atoms in the structure causing the redistribution of lone pair surrounding carbon atoms (Figure 4e and f).[70,109,110] Albeit the vacancy location cannot be figured out by using EPR alone, most of the studies employed this method as a complementary to aforementioned techniques.[64,94,99,110–112] Nevertheless, certain pioneering studies employing pulsed dipolar and hyperfine spectroscopies have unveiled the precise positioning of two radical pairs, approximately 2 nm apart (equivalent to roughly four tri-s-triazine moieties). For a more in-depth understanding of the measurements conducted with EPR and related techniques, we recommend consulting the following articles.[113,114]

Moreover, the re-organization of the heptazine motifs might cause not only the distortion in π-π conjugation but also new appearing polar functional groups. For this purpose, ***Fourier transform infrared spectroscopy (FTIR)*** plays a crucial role since different reagents and conditions might lead to distinct defects whether cyano, amino or other types. In FTIR, molecular vibrations resemble to the oscillations of a spring, and the intensity of the absorption bands is directly related to the strength of the bonds and the masses involved, according to the Hooke's Law.[115] The typical structural features of CN were assigned as the sharp peak in the region around 812 cm^{-1}, corresponding to the stretching vibrations of C=N bonds, which are intrinsic to the heptazine units in the CN lattice. The peaks in the 900–1800 cm^{-1} range are associated with the bending vibrations of bridging N–H bonds or C–N=C units. Additionally, the broad absorption band in the range of 3000–3500 cm^{-1} signifies the stretching vibrations of $-NH_x$, reflecting the presence of amino groups, showing incomplete polymerization.[73] Niu *et al.* observed a slight shift (ca. 5 cm^{-1}) to lower frequency for the peaks below 2000 cm^{-1} in the FTIR spectrum of CN after the generation of N-vacancies and it was considered the fully condensation of CN owing to the loss of sp^3 N-bridging atoms (NH_x).[46] Different strategies resulted in the functional groups mainly cyano,[76,92,116] amino[56,117–119] and imine-like groups[120] in the heptazine rings while the disappearance of the peak at 812 cm^{-1} was also observed (Figure 5a and b).[48,76] Furthermore, the emergence of a new peak in the range of 1000–1200 cm^{-1} is attributed to the creation of C–O bonds, a consequence of the treatment conditions designed to introduce oxygen-containing functional groups.[80,121]

Solid State Nuclear Magnetic Resonance (ssNMR) Spectroscopy is another efficient analytical tools to investigate the vacancies in CN structures.[122–124] Due to low abundance of ^{13}C and ^{15}N, cross-polarization (CP) experiments, which is a technique used to enhance the signals from nuclei with low sensitivity (like ^{13}C) by transferring polarization from nearby nuclei with higher sensitivity (usually ^{1}H), have risen in recent years. Thanks to Schnick's studies on the understanding of important intermediates while thermal condensation, there is a guidance to interpret the noncrystalline CN and the changes in its skeleton.[73,125] The peaks appearing at 157 ppm (C_i) and 165 ppm (C_e) of melem are also the most characteristic peaks that of CN. For a typical ^{13}C CP MAS NMR spectrum, C_e signals are expected to be more intense owing to their close spatial distance to unreacted-NH_x groups.[125] Albeit the quantification of the peak intensities cannot relate the ratio of moieties in CN structure, it might give some clue for their abundance. The chosen synthetic strategy might lead to different structural changes and alteration of the signal intensity, thus indicating the amount of $-NH_x$ groups or functional groups has changed. For example, the decrease intensity of peak at 156–157 ppm belonging to C_i is attributed to the created N_{2C} vacancies in the structure[116,121,126] or the increased area of C_e is interpreted as the addition of H-bond containing functional groups might strength the area of that corresponding signals[59] and those peaks were compared in some cases (Figure 5c).[75,83,112,121,126,127] In addition to that, the broadness and the new appearing shoulders on these characteristic peaks show the disordered melem units in CN structure after the introduction of *N*-vacancies.[77,99,100,128] The alteration in the chemical shift of those related signals towards downfield or upfield provides an additional information about the origin of the generated defects in the structure. In our recent study about the photocatalysis of N-vacancy CN, C_i and C_e experienced a shift towards a higher magnetic field due to the presence of N-vacancies, which disrupted the spread of electrons in the aromatic system.[59] This change in the chemical shift was attributed to the formation of imine-like features in tri-s-triazine rings. Certain instances, electron rich environment was observed and caused the shielding effect after the introduction of N-related defects in melem motifs.[48,77,102] Besides these traditional peaks, C_i and C_e, new peaks appeared and associated with electron withdrawing substituents such as cyano,[92,111,129] amide,[65] etc.[98] (Figure 5d). To make a long story short, one can get very insightful information from just these two peaks. Moreover, ^{15}N CP MAS and ^{1}H MAS NMR are also useful techniques to distinguished between the different forms of the produced CN. The similar explanations in which the distance of protons causing the peak intensity are encountered in the case of ^{15}N CP MAS NMR as well.[73,125] Due to low abundance (0.37%) and gyromagnetic ratio of ^{15}N, only after the CP MAS NMR measurements with ^{15}N labelled-precursors results in smooth signals.[122,130] However, most of the studies investigating N-defects in CN was only considered using ^{13}C CP MAS NMR spectrum. Above and beyond, researchers studied the efficiency of non-elemental doping after the construction of structural

© 2024 The Authors. ChemCatChem published by Wiley-VCH GmbH

18673899, 0, Downloaded from https://chemistry-europe.onlinelibrary.wiley.com/doi/10.1002/cctc.202301560 by Koc University, Wiley Online Library on [12/07/2024]. See the Terms and Conditions (https://onlinelibrary.wiley.com/terms-and-conditions) on Wiley Online Library for rules of use; OA articles are governed by the applicable Creative Commons License

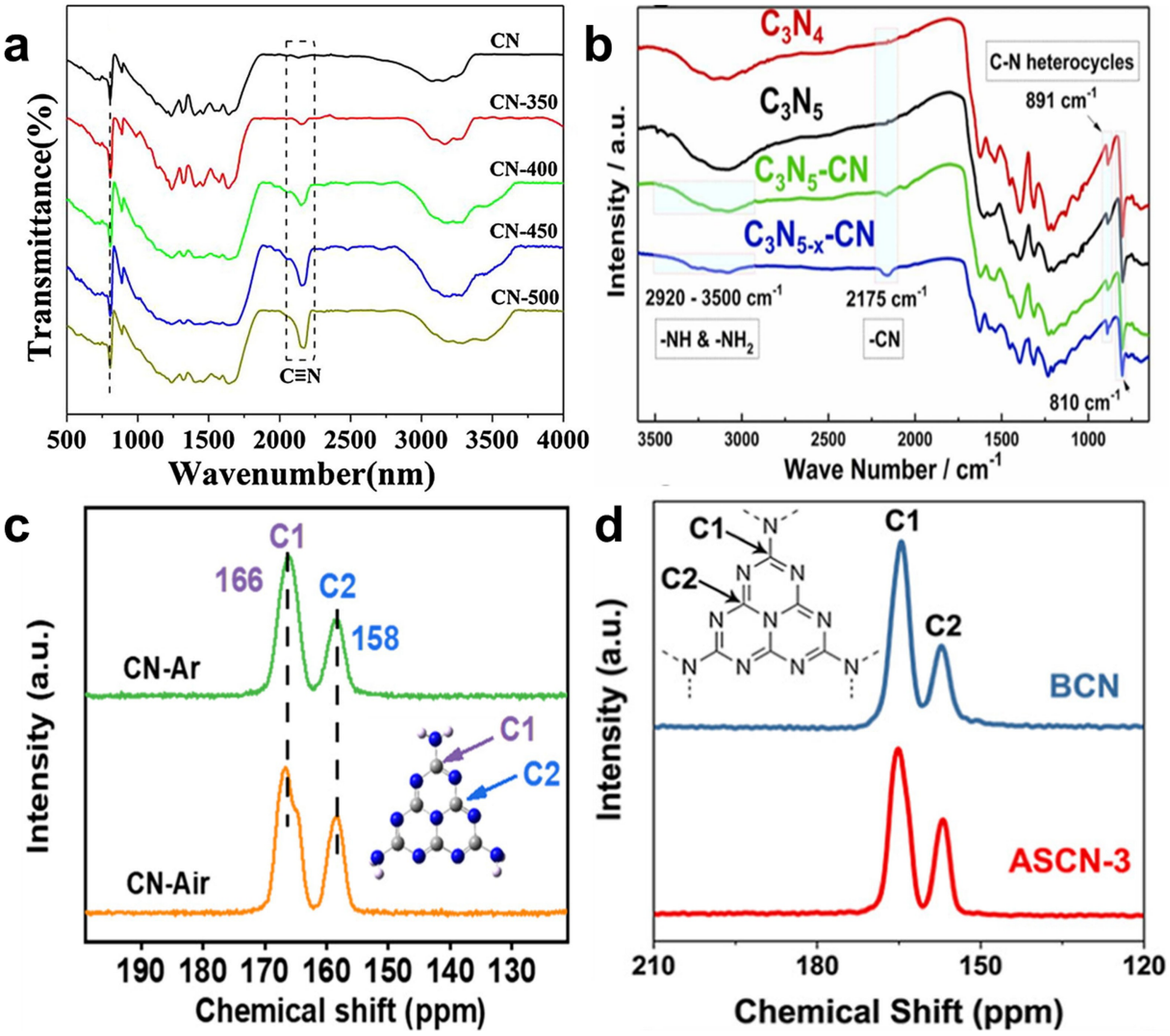


Figure 5. FT-IR spectra of **(a)** CN and CN-T. Reprinted from.[92] Copyright (2019) with permission from Elsevier. **(b)** different catalysts. Reprinted from.[119] Copyright (2023) with permission from Elsevier. Solid-state ^{13}C NMR spectra of **(c)** CN-Air and CN-Ar. Reprinted (adapted) with permission from.[75] Copyright 2023 American Chemical Society. **(e)** BCN and ASCN. Reprinted (adapted) with permission from.[65] Copyright 2023 American Chemical Society.

defects on CN also examined ^{31}P and ^{11}B CP MAS NMR along with ^{13}C CP MAS NMR.

In the case of N-vacancy CNs, **Transmission Electron Microscopy (TEM)** plays a crucial role in providing detailed insights into their morphology, crystallinity, and nanoscale features. In the majority of investigations, a sheet-like morphology, curly edges, broken layers, and newly formed pores resulting from the release of $-NH_x$ fragments during the calcination process, were frequently documented about N-vacancy CNs (Figure 6a).[63,97] The manipulation of various procedures, such as the addition of oxamide[131]/triethanolamine[132] and calcination at elevated temperatures,[78,110] resulted in the rolling up of the edges of CN layers and forming ultra-thin nanosheets. Furthermore, Liu *et al.* integrated their findings from Atomic Force Microscopy (AFM) and TEM to demonstrate that the thickness of CN layers decreased from 1.56 to 0.51 nm as the temperature increased.[110] In another study, an intriguing discovery was reported by Deng *et al.* asserting that the crystallinity of CN was enhanced by the calcination process with no observable alterations in the morphology.[133] The liberation of N-containing fragments in gaseous form tends to give rise to a porous structure, and these pores play crucial roles such as more active sites, enlarged specific surface area, and the defects that enhance the mobility of photogenerated charge carriers.[79,84,134] Most of the studies including ours reported similar morphology changes after the thermal treatment of CN (Figure 6b).[57,59,63,75,135] The utilization of a template during synthesis[85,112] resulted in a thinner structure with homogeneously distributed pores matching with the size of template, whereas diverse conditions yielded varying morphologies such as coral-like,[88] rod-like,[83,136] and spherical[48] structures (Figure 6c). For instance, Nguyen *et al.* discussed the effect of reaction atmospheres including air, N_2, and CO_2 on the synthesis of CN and they reported the formation of smaller pores under CO_2 atmosphere while larger ones in the case of N_2 environment.[79] Yang *et al.* documented a dramatic change in

© 2024 The Authors. ChemCatChem published by Wiley-VCH GmbH

18673899, 0, Downloaded from https://chemistry-europe.onlinelibrary.wiley.com/doi/10.1002/cctc.202301560 by Koc University, Wiley Online Library on [12/07/2024]. See the Terms and Conditions (https://onlinelibrary.wiley.com/terms-and-conditions) on Wiley Online Library for rules of use; OA articles are governed by the applicable Creative Commons License

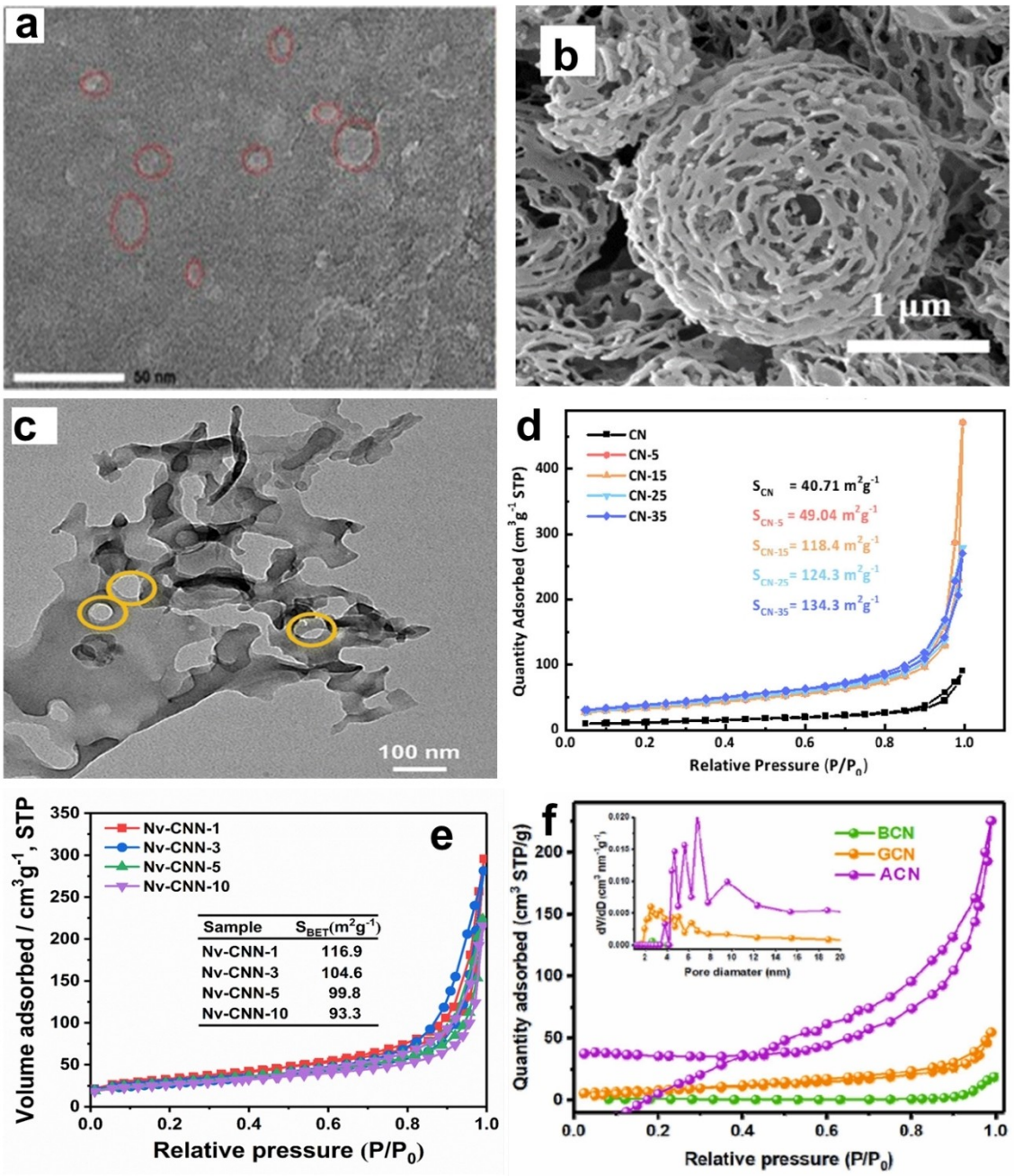


Figure 6. TEM image of **(a)** CN-UNS. Reprinted from[63] Copyright (2022) with permission from Elsevier. **(b)** N-vacancy CN. Reproduced from[59] with permission from the Royal Society of Chemistry. **(c)** CNS. Reprinted from.[48] Copyright (2022) with permission from Elsevier. Nitrogen adsorption–desorption isotherms of **(d)** CN-X and CN. Reprinted (adapted) with permission from.[78] Copyright 2023 American Chemical Society. **(e)** Nv-CNN-1, Nv-CNN-3, Nv-CNN-5 and Nv-CNN-10. Reprinted from.[112] Copyright (2022) with permission from Elsevier. **(f)** BCN, GCN and CAN. Reprinted from.[121] Copyright (2022) with permission from Elsevier.

the morphology of CN from macroporous to mesoporous structure in the presence of triethanolamine as an additive during the synthesis.[132] On a related note, Gholipour and co-workers suggested that noticeable voids in the 2D nanosheets not only serve as active sites but also introduce new defect levels to the bandgap (midgap states) of N-vacancy CN.[117]

The porous structure obtained was typically correlated with the data from ***Gas Adsorption-Desorption Analysis*** to assemble additional insights into surface properties such as surface area and pore volume/size. Huang *et al.* devised a synthesis method that incorporated various precursors in the presence of KOH and explored the outcomes of their combinations.[134] The inclusion of KOH during calcination yielded a distinctive flower-like structure with a mesoporous surface. While the techniques based on electron microscopy enables the visualization of porous structures, crucial surface properties like specific surface area and pore volume remain elusive through this technique. Gas adsorption-desorption measurements, particularly utilizing

© 2024 The Authors. ChemCatChem published by Wiley-VCH GmbH

18673899, 0, Downloaded from https://chemistry-europe.onlinelibrary.wiley.com/doi/10.1002/cctc.202301560 by Koc University, Wiley Online Library on [12/07/2024]. See the Terms and Conditions (https://onlinelibrary.wiley.com/terms-and-conditions) on Wiley Online Library for rules of use; OA articles are governed by the applicable Creative Commons License

18673899, 0, Downloaded from https://chemistry-europe.onlinelibrary.wiley.com/doi/10.1002/cctc.202301560 by Koc University, Wiley Online Library on [12/07/2024]. See the Terms and Conditions (https://onlinelibrary.wiley.com/terms-and-conditions) on Wiley Online Library for rules of use; OA articles are governed by the applicable Creative Commons License

nitrogen gas, emerge as an indispensable tool by quantifying the amount of gas adsorbed on a sample at specific pressure values, providing essential information for a comprehensive understanding of material properties. In most of the studies, defect engineering of a certain material is known to increase the specific surface area of the corresponding material.[5,137] In the case of manipulating the structure of CN with an aim of creating N-vacancies, it was observed that different calcination strategies led to various texture properties. One of the first studies in this manner was the pioneer study of Dong *et al.* showing the correlation between the duration of pyrolysis and the thickness of CN layers.[55] As the outcomes (288 m^2/g vs 31 m^2/g) revealed a notable augmentation in the specific surface area surpassing the standard CN, the investigation predominantly delved into the impacts of time and temperature within this domain. Furthermore, employing steam flow[78] and an argon atmosphere[91] during synthesis led to increased surface areas, particularly with extended calcination periods (Figure 6d). In contrast, Zhao *et al.* reported divergent outcomes in their synthesis approach, which incorporated Pluronic F-127 as a template (Figure 6e).[112] A comparable trend in the enlargement of surface area of CN was reported employing a second calcination at higher temperatures (in the range of 400 to 650 °C).[61,110,138] In contrast, no significant alterations in surface area of CN were reported under various conditions including vacuum technology and alkali-assisted calcination despite increasing temperatures.[64,139] Cheng *et al.* introduced CN using diverse precursors including urea, thiourea, biuret, dicyandiamide, and melamine.[140] They conducted a comparative analysis of their textural properties, revealing that biuret-based CN exhibited superior surface area with relatively small pore size (11.2 nm) and photocatalytic performance. Numerous studies have contributed to the field with utilizing diverse gaseous environments during the synthesis of CN via thermal polycondensation protocol, yielding intriguing and noteworthy results. For example, Lan *et. al.* endeavored to generate N-vacancies within the CN structure by disrupting intralayer hydrogen bonds under a hydrogen gas atmosphere, yielding an increase in the surface area from 9.82 m^2/g to 65.56 m^2/g.[77] In another study, Zhang *et al.* preferred argon gas and air atmosphere for the synthesis of CN and reported a higher specific surface area for the CN prepared under argon gas.[75] Upon the synthesis of CN under the calcination atmospheres including air, N_2, and CO_2 in the presence of thiourea as the precursor, the calculated surface areas of the yielded CN followed the order of air (25.0 m^2/g) > CO_2 (17.9 m^2/g) > N_2 (11.4 m^2/g).[79] Zhang *et. al.* documented a substantial increase in surface area from an initial value of 6.1 m^2/g to a noteworthy 267.1 m^2/g after subjecting CN to multiple rounds of calcination.[62] An alternative method employing an ultra-fast heating system up to 800 °C yielded a CN with a high surface area of 261.2 m^2/g.[63] Additionally, Li *et al.* achieved a surface area of 274.1 m^2/g by introducing an additional carbon source, glucose, during the synthesis of CN.[100] However, a significantly elevated surface area of 405.76 m^2/g, as opposed to 4.89 m^2/g, was attained through the utilization of H_2 plasma treatment, targeting the creation of N-vacancies in CN (Figure 6f).[121]

Positron annihilation spectroscopy (PAS) is a rarely used method to study the N-vacancies in CN. In this technique, positrons are trapped by defects, causing a slowing down in their annihilation.[141,142] The resulting positron annihilation spectrum provides three values (τ values), each corresponding to different defect sizes and locations. It is commonly acknowledged that τ_1 and τ_2 are conventionally ascribed to the positron annihilation lifetime within the intrinsic structure and defects of the crystal, respectively. To the best authors' knowledge, there are only two studies reported in the available literature. In the first example, Praus *et al.* synthesized melamine-based CN and subjected it to post-calcination under static air at 500 °C and under an argon flow at 550 °C. Their investigation with PAS revealed the presence of both carbon and N vacancies with a notably higher generation of voids observed under the argon treatment.[143] In the second study, Zhao *et al.* observed an elevation in both τ_1 and τ_2 values in N-vacancy CN compared to that of its bulk counterpart with PAS analysis.[116] This phenomenon proves the elimination of N atoms in their synthesis strategy, involving the calcination of NaOH and dicyandiamide mixture at 550 °C for 4 h.

Computational calculations offer a precise means to predict the formation energy of vacancies within CN material from a theoretical standpoint. Earlier studies were focused mostly on the unveiling the repeating motifs of CN polymeric structure and some results show the most stable one seems tri-s-triazine unit.[144–147] Following identified limitations, such as high recombination in photocatalytic applications, efforts have been directed toward enhancing the optical properties of CN. This pursuit has concurrently led to an expansion in computational analyses, delving into the chemical and physical characteristics of CN.[148,149] Numerous researchers have devoted considerable effort to employing diverse methodologies, aiming to approach the experimental band structure of CN. Their focus extends to understanding the influence of doping on the electronic properties of CN, as well as investigating the effects of adsorption on active sites within the material.[149] The inclusion of the latter was primarily prompted by the superior photocatalytic activity exhibited by CN. In their study, Wu *et al.* delved into the impact of imperfections in CN on water adsorption,[150] while Raciti *et al.* elucidated the interaction between perfluoroalkyl halides and N-defect CN, highlighting the presence of midgap states in the material.[151] The impact of N-related defects on the adsorption of intermediates during photocatalytic NO_x removal[118] and the generation of reactive oxygen species[152] on CN has been thoroughly examined and proven to be more successful compared to pristine CN. Furthermore, in many instances, the introduction of these defects resulted in the creation of intermediate energy levels, effectively preventing recombination and thereby enhancing the material's light harvesting ability.[132,153–155] To establish a correlation between the vacancy type and its location within the tri-s-triazine unit, as well as its relationship with active sites, researchers conducted calculations to determine the energy levels associated with different possibilities. While some studies suggested that N_{3C} vacancies are more favorable due to their lower formation energy,[132,156] other research argued in favor of the removal of

© 2024 The Authors. ChemCatChem published by Wiley-VCH GmbH

N_{2C} from the heptazine motifs, emphasizing its low energy and high abundance in enhancing photocatalytic processes.[101]

On the other hand, the light-harvesting efficiency of a photocatalyst is linked to its bandgap energy, dictating the minimum photon energy required for absorption.[157] In particular, a semiconductor photocatalyst selectively absorbs photons possessing energy equal to or exceeding its bandgap energy. Following photon absorption, electrons undergo excitation to the higher energy CB, contributing to reduction reactions. At the same time, concurrently, holes are generated in the VB, participating in oxidation reactions.[158] The bandgap energy serves as a critical determinant of the wavelength range over which light is effectively harvested. Semiconductor materials characterized by wide bandgap energies predominantly absorb ultraviolet (UV) light ($\lambda < 420$ nm), constituting merely about 5% of the total solar spectrum.[159] In contrast, semiconductors with narrower bandgap energies exhibit light absorption in the visible ($420 < \lambda < 780$ nm) and near-infrared (NIR) regions ($780 < \lambda < 2500$ nm), which collectively account for approximately 43% and 52% of solar energy, respectively.[160] It is noteworthy that the photophysical properties are not solely governed by bandgap energy but are also influenced by the potential potentials of the semiconductor. Mismatching the VB and CB potentials can impede the overall redox capabilities of the photocatalytic system.[161] CN, with a bandgap of around 2.7 eV, has garnered attention in photocatalytic reactions owing to its favorable VB and CB band potentials.[162] However, the inherent challenges of high recombination and low electron mobility necessitate improvements in its photo(catalytical)physical properties.[163] In 2012, Niu *et al.* reported that the introduction of N-vacancies induced changes in the electronic band structure of CN.[46] UV-Vis absorption spectroscopy analysis identified a novel absorption band spanning 450 to 600 nm in *N*-deficient CN compared to pristine CN. Their optical bandgap calculation by the transformed Kubelka-Munk function revealed a decrease in the optical bandgap from 2.74 to 2.66 eV due to N-vacancies. This promising outcome underscores the transformative impact of N vacancy-induced alterations on the electronic structure of CN, resulting in an expanded light absorption range and enhanced sunlight utilization. Moreover, N-vacancies in CN exhibits a band-to-band PL emission characteristic similar to CN. The significantly diminished emission intensity suggests a notable reduction in the likelihood of radiative recombination of photoexcited charge carriers within N-deficient CN. To corroborate this insight, an examination of the charge carrier lifetimes was conducted by the authors through the recording of time-resolved photoluminescence spectra (TRPL). The fluorescence decay kinetics of N-deficiency in CN were found to be marginally slower compared to those of pristine CN. The observed decline in PL intensity and the dynamic alteration in the percentage of short-lived and long-lived charge carriers are intricately linked to localized states within the band gap, specifically formed after the removal of N atoms from CN skeleton.

To elucidate the sophisticated photophysical characteristics of the synthesized N-vacancy CN photocatalysts a comprehensive examination was undertaken by different researchers. The exploration revealed augmented light-harvesting capabilities and a consequential shift in band potentials as evidenced by UV-vis absorbance spectra. This transformative outcome has given rise to novel conceptual frameworks the same idea with different keywords including midgap states,[63] defect levels,[120] impurity energy levels,[69] intra-gap levels,[164] extinction-mediated trap states,[165] defect states,[48] and electronic vacancies.[110] These emergent concepts represent a significant advancement in our understanding of the photochemical intricacies inherent in N-vacancy CN photocatalysts shedding light on their enhanced performance and paving the way for further advancements in the realm of photocatalysis.

In the investigation focusing on the utilization of N-deficient CN for photocatalytic and piezocatalytic degradation of organic contaminants, the optical properties were systematically probed using UV-vis diffuse reflectance spectroscopy (DRS) and PL spectroscopy (Figure 7a).[96] The acquired samples exhibited pronounced absorption characteristics within the 300–450 nm range, showcasing the influence of N-defects. A comparative analysis between N-deficient CN samples and pristine CN revealed a notable red shift in the absorption band edge. This shift was correlated with the extension of annealing time in a nitrogen atmosphere and the emergence of N-defects within the CN lattice. Furthermore, examination of Tauc plots indicated a reduction in the bandgap energy from 2.84 to 2.80 as the prevalence of N-defects increased. Furthermore, in the PL spectrum, the emission intensity of N-vacancy samples was observed to be lower than that of pristine CN, attributing this reduction to a decreased recombination rate of photoexcited carriers in these samples. It was additionally noted that the carrier recombination rate increased when the annealing duration exceeded 6 h. Cong *et al.* observed a discernible red shift in the UV-vis DRS spectra of their oxygen-modified N-deficient CN.[95] This observation was underscored by the concurrent presence of N-vacancies and oxygen-containing functional groups. Specifically, the interaction of a lone electron pair within the defect region facilitated the $n \rightarrow \pi^*$ electronic transition, contributing to the observed red shift in the DRS spectra. Upon inspection of the PL spectrum, a notable distinction emerged between pristine CN and N-vacancy CN samples. While pristine CN exhibited a robust luminescence intensity, the luminescence intensity of N-vacancy CN markedly diminished. This phenomenon was attributed to the tendency of the N-defect regions to trap photogenerated electrons, leading to restricted recombination of photoinduced electrons and holes. Upon scrutinizing the DRS and bandgaps of N-deficient CN, synthesized through alkali-assisted thermal polymerization of urea, a systematic redshift at the absorption edge was discerned with an escalating utilization of KOH (Figure 7b).[98] This observed phenomenon was ascribed to the achievement of a homogenous distribution of N-defects throughout the material's bulk. Furthermore, an assessment of the bandgaps derived from the transformed Kubelka-Munk function revealed a noteworthy reduction from 2.68 to 2.36 eV. This reduction in band gaps signifies a structural modulation induced by the alkali-assisted synthesis process, suggesting a potential avenue for tailoring the electronic properties of N-

© 2024 The Authors. ChemCatChem published by Wiley-VCH GmbH

18673899, 0, Downloaded from https://chemistry-europe.onlinelibrary.wiley.com/doi/10.1002/cctc.202301560 by Koc University, Wiley Online Library on [12/07/2024]. See the Terms and Conditions (https://onlinelibrary.wiley.com/terms-and-conditions) on Wiley Online Library for rules of use; OA articles are governed by the applicable Creative Commons License

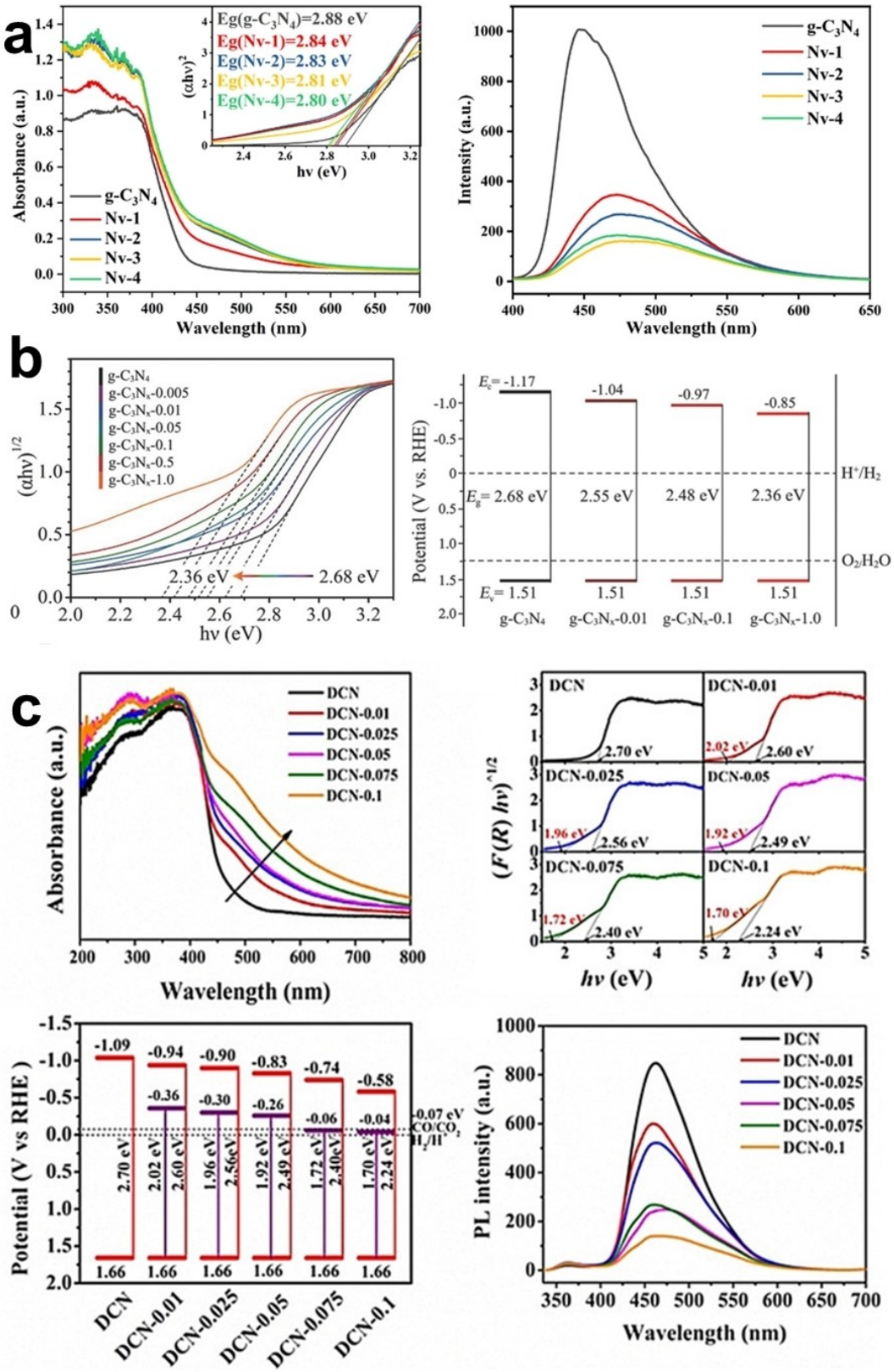


Figure 7. (a) UV-vis DRS, PL spectra for g-C_3N_4 and Nv-x (x = 1, 2, 3, 4) samples. The inset of includes Tauc plots. Reproduced with permission from[96] Copyright 2021 Springer Nature. **(b)** Graphs depicting the transformed Kubelka–Munk function versus photon energy and band potentials for g-C_3N_4 and g-C_3N_x. Reproduced with permission.[98] Copyright 2017, Wiley. **(c)** UV/Vis DRS, Tauc Plots, Band alignments and steady-state PL spectra for DCN and DCN-x. Reproduced with permission.[81] Copyright 2019, Wiley.

© 2024 The Authors. ChemCatChem published by Wiley-VCH GmbH

18673899, 0, Downloaded from https://chemistry-europe.onlinelibrary.wiley.com/doi/10.1002/cctc.202301560 by Koc University, Wiley Online Library on [12/07/2024]. See the Terms and Conditions (https://onlinelibrary.wiley.com/terms-and-conditions) on Wiley Online Library for rules of use; OA articles are governed by the applicable Creative Commons License

deficient CN materials. Moreover, in investigating the role of photoexcited charge carriers associated with N-vacancy CN, a distinctive trend was noted. Specifically, the PL emission exhibited a gradual reduction in intensity and a concurrent red shift when KOH was introduced during the thermal polymerization process in comparison to pristine CN. Through the application of thermal vacuum technology, the synthesis of central N-vacancies in CN revealed a notable expansion in the absorbance spectrum.[64] This expansion was attributed to the introduction of central N-vacancies within the material. Concurrently, an observed reduction in the bandgap from 2.73 eV to 2.65 eV was documented. The observed reduction in PL and TRPL spectra in N-vacancy CN, in comparison to pristine CN, is indicative of a concurrent decrease in charge recombination and an improvement in charge separation. In the investigations involving the synthesis of N-vacancy CN utilizing peanut oil,[71] glucose,[100] and ammonium acetate[97] as additives, notable findings were observed. Specifically, it was reported that the edges of the light absorption band exhibited a discernible redshift, indicative of a modification in the material's optical properties. Moreover, a consequential expansion in the light absorption range of the photocatalyst was identified when compared to pristine CN. Additionally, through an analysis of charge dynamics, a discernible reduction in the recombination rate and a concurrent increase in the separation of photo-induced electrons and holes were elucidated.

Beyond the augmentation of the material's light absorption capacity, and the consequential red shift in band edges, the creation of novel states between VB and CB as well as their identification stand out as crucial aspects in elucidating the photocatalytic activity-mechanism relationship. The establishment of these new states assumes significance in understanding the intricate mechanisms underlying the enhanced performance of the material. In 2018, Shi *et al.* reported the confirmation of trapped states associated with N-vacancies in CN through DRS, PL, TRPL, and transient absorption measurements (Figure 7c).[81] The DRS spectrum revealed a distinct absorption tail in the visible region, indicating the presence of these trapped states. Additionally, the Tauc plot unveiled the emergence of a second bandgap, showcasing the complex electronic structure of the material. The observed reduction in band gaps from 2.7 eV to 2.24 eV was attributed to the introduction of N vacancies in CN structure. This reduction not only amplified visible light absorption but also introduced a defect level, inducing transformative changes in the electron structure of CN. Moreover, the appearance of a second bandgap at 1.70 eV emphasized the complex interplay between N-vacancies and the electronic properties of CN. PL and TRPL analyses were systematically conducted to scrutinize the charge separation dynamics in N-deficient CN. In both analyses, a notable decrease in signal intensity was observed, indicating a pronounced suppression of light-induced recombination between electrons and holes. The photocatalyst synthesized through plasma-tuned N-vacancy CN sphere formation exhibited markedly enhanced light-absorption capabilities compared to pristine CN across visible and UV regions.[48] Notably, the absorption edge in the visible light spectrum experienced a substantial increase at approximately 670 nm, attributed to the formation of N-vacancies. PL spectra of the synthesized materials exhibited a discernible reduction in emission peak intensity when compared to pristine CN. This phenomenon suggests that the formation of N-vacancies effectively impedes charge recombination processes. In the case of N-vacancy CN synthesized by Tu and collaborators via the two-step calcination method, a notable enhancement in the visible light absorption was observed, which was characterized by a broad shoulder tail known as the Urbach tail in the absorption spectra.[24] Simultaneously, a gradual red shift in the visible light range was noted, correlating with an increased density of N-vacancies along the edge of the Urbach tail. Typically, the Urbach tail is associated with electronic states situated within the band gap, referred to as midgap states.[166,167] In their study, Tu *et al.* delved into the electronic structure of CN nanosheets incorporating N-vacancies using periodic density functional theory (DFT). Interestingly, the calculated band gap for pristine CN was determined to be 1.03 eV, a value notably smaller than the experimental counterpart (2.7 eV). To further examine this discrepancy, Urbach plots were employed to identify midgap states which are located between the VB and CB. In the PL spectrum, a discernible trend is observed wherein the emission intensity diminishes with an increasing density of N-vacancies. The reduction observed in emission intensity signifies a concomitant decrease in the recombination of photogenerated electron-hole pairs when compared to pristine CN. The emergence of a distinctive absorption edge between 420 and 550 nm in the absorption spectrum of N-vacancy CN, tailored by our research group for visible-light-driven oxidative Mannich reactions, is interpreted as indicative of the presence of a midgap states.[59] This newly observed feature in the absorption profile suggests the introduction of electronic states between the VB and CB levels, signifying the alteration in the electronic structure induced by the incorporation of N-vacancies. Furthermore, in our comprehensive analysis of charge separation dynamics, the concurrent decrease in both PL and TRPL intensities serve as an indicative measure of diminished recombination and improved charge separation. The existence of midgap states in N-vacancy CN synthesized through diverse methods including thermal condensation utilizing a covered ceramic arc,[133] acetamide- or formamide-assisted in situ approaches,[99] a three-step thermal exfoliation method,[62] polycondensation using RUB-15 template,[168] and Molten salt-assisted method[169] has been verified. Additionally, the impact of these midgap states on the photocatalytic activity of CN was carefully investigated. In a noteworthy investigation done by Xue *et al.* in 2019, the band potential characteristics of N-vacancy CN synthesized through the KOH-assisted thermal polymerization method were thoroughly examined.[94] This study revealed intriguing alterations in the absorbance spectrum of CN, including a shift of the intrinsic absorption edge to approximately 500 nm. Particularly noteworthy was the observation of a noticeable shoulder extending down to ~700 nm, thus further extending the absorption profile of N-defective CN. This shoulder that is elucidated to possess a bandgap of ~2.70 eV with a sub-bandgap of ~1.88 eV corresponding to the

© 2024 The Authors. ChemCatChem published by Wiley-VCH GmbH

18673899, 0, Downloaded from https://chemistry-europe.onlinelibrary.wiley.com/doi/10.1002/cctc.202301560 by Koc University, Wiley Online Library on [12/07/2024]. See the Terms and Conditions (https://onlinelibrary.wiley.com/terms-and-conditions) on Wiley Online Library for rules of use; OA articles are governed by the applicable Creative Commons License

absorption edge introduces a significant aspect to the optical properties of CN. XPS-VB results complemented these findings, indicating the emergence of two continuum states for N-vacancy, overlapping with the VB edge. Notably, a tail state close to the VB was identified as shown in Figure 8.[94]

Explorations into the alterations of photophysical properties covering absorbance capacity, absorption edges, bandgap, and dynamics of photoexcited charge separation attributed to N-vacancy formation in CN have been conducted by using various techniques beyond those mentioned earlier. These techniques such as transient absorption spectroscopy,[81,95] steady-state and transient-state surface photovoltage (TS-SPV),[64] photocurrent,[24] and electrochemical impedance spectroscopy (EIS)[48] have provided valuable insights into the photophysical characteristics of N-vacancy CN. Positive findings include enhanced production rates of photogenerated electrons, reduced recombination rates, improved migration kinetics, and increased carrier separation. These versatile studies provide a holistic understanding of the complex relation of N-vacancies with the photophysical properties of CN, which is the topic of next chapter.

5. Relationship Status: Bridging the Gap Between Defects and Photocatalytic Performance

The exploration of the impact of N-vacancies in CN, specifically in relation to optical properties and their correlation with improvements in associated photoredox transformations, remains an ongoing curiosity (Table 1). In a particular study, the influence of an inert atmosphere, specifically argon gas, during the calcination process was investigated.[143] The study interpreted the creation of substantial vacancies, attributing it to the divergent flow of gas molecules, ammonia, and argon, as opposed to the conditions in static air. The vacancy types were meticulously identified through PAS analysis, establishing a correlation with the enhanced photocatalytic activity observed in CN subjected to calcination under argon for a duration of 3 h. Xie *et al.* incorporated KOH in varying amounts and subjected urea-based CN to calcination at 500 °C for 2 h.[170] The optimal additive content was determined by comparing the generated *N*-vacancies and their types in the structure. NH_x vacancies were attributed to the enhancement of photogenerated charge carriers, leading to an increased oxygen reduction. Conversely, Shiraishi and colleagues observed that NH_x

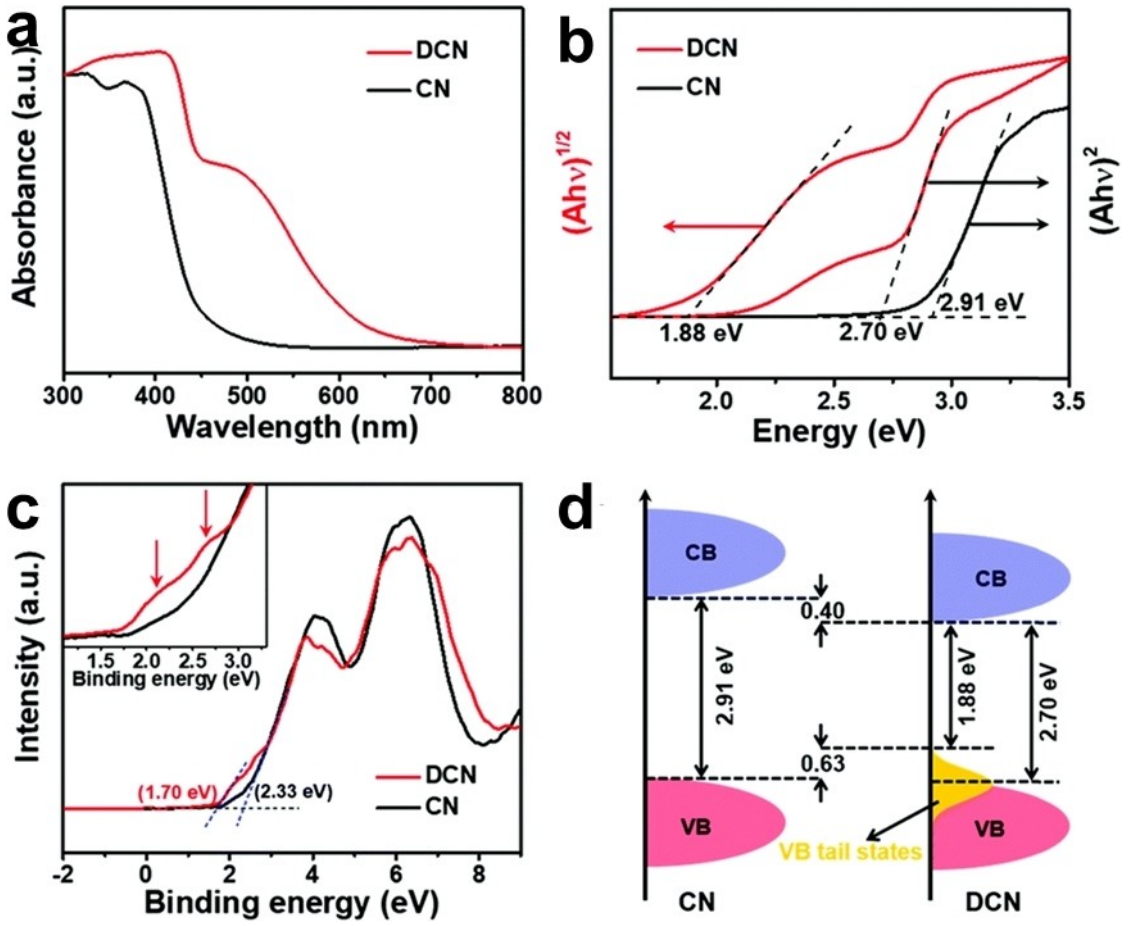


Figure 8. **(a)** UV/Vis DRS, **(b)** Tauc Plots, **(c)** VB-XPS spectra and **(d)** Band alignments for CN and DCN. Reproduced from[94] with permission from the Royal Society of Chemistry.

© 2024 The Authors. ChemCatChem published by Wiley-VCH GmbH

18673899, 0, Downloaded from https://chemistry-europe.onlinelibrary.wiley.com/doi/10.1002/cctc.202301560 by Koc University, Wiley Online Library on [12/07/2024]. See the Terms and Conditions (https://onlinelibrary.wiley.com/terms-and-conditions) on Wiley Online Library for rules of use; OA articles are governed by the applicable Creative Commons License

Review
doi.org/10.1002/cctc.202301560

Chemistry Europe
European Chemical Societies Publishing

Table 1. Summary of the relationship between defects and photocatalytic performance.

Catalyst	Synthesis method & precursors	Characterization of catalyst	Light sources	Application	Comments	Ref
GCN(*x*)	Thermal polycondensation with N_2 flow & cyanamide, Ludox HS40	UV-vis DRS, XRD, XPS, ESR, TEM, LSV, BET	2 kW Xe lamp	H_2O_2 production	Conduction band electrons localized at the1,4-positions of the melem unit promote two-electron ORR	[171]
CN-X	Two-step calcination with H_2 atmosphere at different temperatures & melamine	UV-vis DRS, PL, XRD, FTIR, XPS, EPR, TEM, BET	300 W Xe lamp $\lambda > 400$ nm	H_2 evolution and CO_2 reduction	Introduced midgap states could become recombination centers	[24]
A-g-C_3N_4	Two-step calcination under an Ar flow & urea	XRD, BET, elemental analysis, FTIR, UV-vis DRS, XPS, TEM, photocurrent	Monochromatic LED lamp (365 nm, 410 nm, or 450 nm)	Nitro reduction	Narrow band gap but H atoms binds strongly to N-defect CN during reduction	[25]
VN-SCN	Plasma treatment with H_2S atmosphere & dicyandiamide	UV-vis DRS, PL, XRD, SEM, XPS, TEM, BET	A 250 W high-pressure Na lamp ($800 > \lambda > 400$ nm)	N_2 fixation	Boosting visible light harvesting ability	[47]
CKCN-M	Two-step calcination with Ar atmosphere & melamine, KOH	UV-vis DRS, PL, OEA, XRD, FTIR, XPS, EPR SEM, TEM, Mott-Schottky, BET	Simulated sunlight AM1.5 (56.8 mW/cm^2)	H_2O_2 evolution	The two types of cooperative nitrogen vacancies	[170]
am-CN	Two-step calcination under an Ar flow & melamine	TEM, HRTEM, Raman, XRD, XPS, UV-vis DRS,	Blue LEDs (450 nm)	Perfluoroalkylation	The effect f N-vacancy on perfluoroalkyl halides and their adsorption	[176]
HCN	Hydrogenation treatment & dicyandiamide	ssNMR	300 W Xe lamp $\lambda > 400$ nm	Water splitting	Amino defect increased the amount of adsorbed water on surface	[175]
CN–Ty, CNCYx	Thermal polymerization method & thiourea/melamine trithiocyanuric acid	XRD, EPR, FTIR, TEM, SEM, UV-vis DRS, PL, TRPL, ssNMR, BET	400 mW/cm^2 white LED	Selective epoxidation of styrene	The effect of spatial structure in photocatalytic epoxidation of styrene	[152]
NDCN	Thermal polycondensation & melamine, NaOH	UV-vis DRS, PL, XRD, FTIR, XPS, ESR SEM,	300 W Xe lamp	H_2O_2 Production	The introduced N_V has effects of oxidation, reduction, and charge recombination.	[172]
ACN	Thermal polycondensation & urea, ammonium acetate	UV-vis DRS, PL, TRPL, XRD, FTIR, XPS, ESR, TEM, BET, Photocurrent	150 W tungsten halogen lamp	NO oxidation	The existence of N_{3C} vacancies in ACN can boost photocatalytic activity.	[174]
Nv-X	Two-step calcination under a flow of N_2 at different time & urea	UV-vis DRS, PL, XRD, FTIR, XPS, SEM, AFM	300 W Xe lamp $\lambda > 400$ nm	Degradation of organic pollutants	The excess amount of defects may increase recombination	[96]
NV-CN, CN/NV-(m)- PCN	Two-step calcination under Ar atmosphere & thiocyanuric acid	XRD, BET, FTIR, *in situ* DRIFT, UV-vis DRS, OEA, XPS, EPR, Mott-Schottky, EIS	White LED (400 mW cm^{-2})	Photo-purification of styrene oxide	Different adsorption sites in N-vacancy CN lead to selective separation	[91]
CN-Ar	Two-step calcination with Ar atmosphere at different temperature & melamine	UV-vis DRS, PL, Elemental analysis, XRD, FTIR, XPS, SEM, Mott-Schottky, PAS, Physisorption of nitrogen	Batch photoreactor with 8 W Hg lamp	Hydrogen generation	The presence of carbon and nitrogen vacancies grouped in their big complexes	[143]
Nv-M	Thermal polycondensation & urea, KOH	UV-vis DRS, PL, TRPL, EIS, XRD, FTIR, XPS, EPR, SEM, BET, ssNMR, Photocurrent	300 W Xe lamp	H_2O_2 generation	Newly created active sites in N-vacancy CN for O_2 adsorption	[173]
CN-Air, CN-Ar	Calcination under Ar and air condition & melamine, cyanuric acid	XRD, EPR, FTIR, TEM, SEM, UV-vis DRS, PL, TRPL, EIS, ssNMR, BET, Mott-Schottky	10 W blue LED lamp ($\lambda = 420$–430 nm)	H_2O_2 production and propylene epoxidation	*in situ* photogenerated H_2O_2 in propylene epoxidation,	[75]
ASCN	Two-step calcination under a flow of N_2 & melamine, L-cysteine	XRD, EPR, FTIR, TEM, SEM, UV-vis DRS, PL, TRPL, EIS, ssNMR, BET, Ultraviolet Photoelectron Spectroscopy, TGA, TS-SPV	300 W Xe lamp	H_2O_2 Production Coupled with Selective Alcohol Oxidation	N_V as oxygen adsorption active site traps electrons to form a superoxide radical	[65]

© 2024 The Authors. ChemCatChem published by Wiley-VCH GmbH

18673899, 0, Downloaded from https://chemistry-europe.onlinelibrary.wiley.com/doi/10.1002/cctc.202301560 by Kor University, Wiley Online Library on [12/07/2024]. See the Terms and Conditions (https://onlinelibrary.wiley.com/terms-and-conditions) on Wiley Online Library for rules of use; OA articles are governed by the applicable Creative Commons License

Table 1. continued

Catalyst	Synthesis method & precursors	Characterization of catalyst	Light sources	Application	Comments	Ref
DxU10-x-1, DxU10-x-2	Two-step calcination under an Ar atmosphere & mixture of dicyandiamide and urea	XRD, elemental analysis, FTIR, BET, UV-vis DRS, XPS, ssNMR, EPR	Xe arc lamp	Cleavage of C–C bond in lignin	The created defect sites can promote the generation of essential reactive radicals and radical intermediates.	[138]

defects decreased the production of H_2O_2 due to their basic nature in their strategy using N-vacancy CN.[171] Using a silica-templated defect engineering strategy, they observed a decrease in activity with an increase in surface area. They attributed this phenomenon to the formation of NH_x moieties on the edges, which resulted in the decomposition of H_2O_2. In a parallel vein, the investigations by Luo *et al.* and Li *et al.* explored the two-electron reduction of oxygen as facilitated by N-vacancy CN, leading to the production of H_2O_2.[47,172,173] In alignment with Shiraishi's discoveries, these studies underscored the pivotal contribution of singlet oxygen ($^1O_2$), albeit with nuanced distinctions in their respective synthesis methodologies.

Additionally, the second type of defect, N_{2C}, played a crucial role in further activating O_2, facilitating the formation of H_2O_2 through a transfer of $2e^-$ and $2H^+$. Duan *et al.* employed in situ diffuse reflectance infrared Fourier transform spectroscopy (DRIFTS) to establish a robust correlation between photocatalytic NO_x removal and the generation of N-defects in CN.[174] Their findings reveal a quantitative increase in crucial reactive oxygen species, such as $^1O_2$ and the superoxide radical ($\bullet O_2^-$), both of which play a pivotal role in the studied application. Moreover, the transformation of NO_2 to NO_3^- was facilitated by active sites formed through N-bridging vacancies in CN, overcoming the required energy barrier (Figure 9a). The amount of missing N atoms in CN and the effect on the corresponding transformation were discussed by Tu *et al.* and Liu *et al.* In the preceding investigation, melamine-based CN underwent treatment in a hydrogen atmosphere at temperatures ranging from 475 to 550 °C.[24] As the temperature increased, a rise in N-defects was discerned through EPR, and a concurrent deepening of midgap states positions in relation to the CB was identified. The excess removal of N atoms was noted as a drawback because they act as recombination centers, particularly when its distance from CB increased. Consequently, the researchers examined these N-deficient CN derivatives, determining the optimal temperature for enhanced photocatalytic activity in CO_2 reduction and hydrogen evolution reaction to be 525 °C. In addition to an elevation in the population of photogenerated electrons, the introduced N-vacancies also played a crucial role in anchoring Pt nanoparticles on the surface of CN (Figure 9b). Conversely, another study highlighted that the incorporation of N-defects in CN leads to a reduction in its piezoelectric properties.[96] Despite this, these defects function as effective exciton trapping centers, promoting the efficient separation of carriers during the photocatalytic process of photodegradation. To validate this phenomenon, the study highlighted the crucial role of annealing duration in optimizing the nitrogen content in CN, which was investigated by monitoring the PL peak intensities. The results demonstrated that an excess of N-defects leads to the formation of new centers, inducing the recombination of photogenerated charge carriers. Wang and colleagues have made a substantial contribution to the literature by investigating the impact of N-vacancies on water splitting through ssNMR.[175] In addition to amino defect CN derived from dicyanamide through hydrogenation, they synthesized urea-based CN at temperatures of

© 2024 The Authors. ChemCatChem published by Wiley-VCH GmbH

18673899, 0, Downloaded from https://chemistry-europe.onlinelibrary.wiley.com/doi/10.1002/cctc.202301560 by Koc University, Wiley Online Library on [12/07/2024]. See the Terms and Conditions (https://onlinelibrary.wiley.com/terms-and-conditions) on Wiley Online Library for rules of use; OA articles are governed by the applicable Creative Commons License

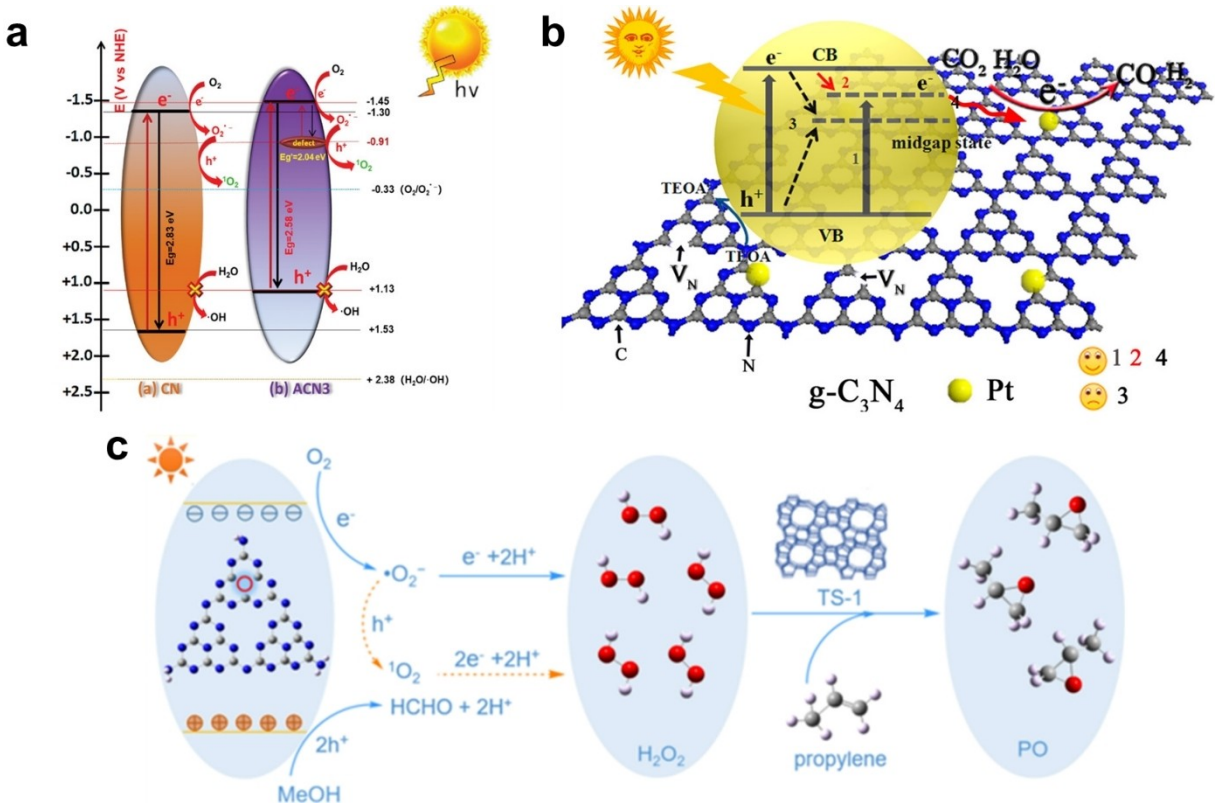


Figure 9. (a) Illustrative representation of the band structure of CN and ACN3. Reproduced with permission.[174] Copyright 2021, Wiley. **(b)** Diagrammatic representation of g-C_3N_4 with N vacancies facilitating the photoreduction of CO_2 to CO and H_2 evolution. Paths 1, 2, and 4 denote the electron excitation from VB to midgap states, the electron trapping from the conduction band to midgap states, and the electron transfer to reaction sites, respectively. Path 3 signifies deeper midgap states serving as recombination sites for trapping photogenerated electrons and holes.[24] **(c)** Diagram illustrating the reaction mechanism for the photocatalytic synthesis of PO using CN-Ar. Reprinted (adapted) with permission from.[75] Copyright 2023 American Chemical Society.

300, 400, 500, and 600 °C. Based on the TGA and differential scanning calorimetry (DSC) results, it was deduced that CN, when calcined at 300 °C, existed in a pre-polymer form, with rearrangement of the structure occurring after reaching 500 °C in the CN structure. The photocatalytic efficiency for the hydrogen evolution reaction decreased with increasing temperature, especially post-600 °C, attributed to partial defects within the repeating units. Remarkably, amino defect-CN, synthesized through hydrogenation, exhibited a significant boost in photocatalytic activity, producing a higher volume of hydrogen gas experiencing an increase from 24 to 424 μmol compared to pristine CN. To elucidate the proximity of defects to active sites in Pt-anchored CN, researchers subjected it to D_2O treatment and conducted specific ssNMR experiments. Under simulated water splitting conditions, the ^1H-^{13}C heteronuclear chemical-shift correlation experiment revealed that the amino defect heightened the hydrophilic nature of the CN structure. This led to increased water uptake, facilitating hydrogen bonding with water molecules. In another study, Zhang and colleagues strategically introduced N_{3C} vacancies into the CN framework to achieve simultaneous production of H_2O_2 and selective formation of propylene oxide.[75] Within their system, they established a correlation between the deficiency-type and the increased quantity of $\bullet O_2^-$, resulting in heightened hydrogen peroxide generation and its subsequent oxidation to $^1O_2$ (Figure 9c). Concurrently, Li and collaborators utilized CN featuring N vacancies and carbonyl groups in the oxygen reduction to H_2O_2 and oxidation of benzyl alcohol derivatives.[65] The identified defects and polar functional groups were discovered to play pivotal roles in the reaction mechanism. Notably, the heightened adsorption capacity was linked to the vacancies, serving to stabilize crucial reactive oxygen species intermediates during the photocatalytic process.

With the aim of advancing the field of selective photooxidation, Tan *et al.* conducted the epoxidation of styrene using N-vacancy CN calcinated at 680 °C, achieving a 65% yield of styrene oxide at 60 °C for 24 hours under visible light conditions.[152] The researchers delved into the potential spatial configurations of the structure and their impact on selectivity. Through DFT calculations and *in situ* FTIR, their findings indicated that the structural configuration interacts with $^1O_2$ and peroxyl species, effectively inhibiting the formation of $^\bullet$OH and H_2O_2 and ultimately contributing to enhanced selectivity. Pursuing a shared objective of achieving high epoxidation selectivity while specifically eliminating benzaldehyde from the reaction mixture, Liu and collaborators employed N-vacancy CN.[91] Their investigation revealed distinctive active sites in N-defect CN for styrene oxide and benzaldehyde, with $^\bullet$OH and H_2O_2 species exclusively forming around benzaldehyde. Notably, the photodegradation of benzaldehyde surpassed >99%

© 2024 The Authors. ChemCatChem published by Wiley-VCH GmbH

18673899, 0, Downloaded from https://chemistry-europe.onlinelibrary.wiley.com/doi/10.1002/cctc.202301560 by Koc University, Wiley Online Library on [12/07/2024]. See the Terms and Conditions (https://onlinelibrary.wiley.com/terms-and-conditions) on Wiley Online Library for rules of use; OA articles are governed by the applicable Creative Commons License

18673899, 0, Downloaded from https://chemistry-europe.onlinelibrary.wiley.com/doi/10.1002/cctc.202301560 by Koc University, Wiley Online Library on [12/07/2024]. See the Terms and Conditions (https://onlinelibrary.wiley.com/terms-and-conditions) on Wiley Online Library for rules of use; OA articles are governed by the applicable Creative Commons License

through this approach. In addition to engaging in bond construction and selective degradation, Cao *et al.* harnessed N-vacancy CN for bond cleavage reactions aimed at converting lignin into value-added products.[138] Drawing from their calculations and experimental results, they proposed the existence of multiple defect sites on N-vacancy CN that interact at the atomic level through σ/π bonds and H-bonding. This structural variability was identified as a key factor contributing to differences in selectivity.

Another noteworthy contribution to photoredox organic chemistry in this field was made by Filippini and co-workers, who explored the impact of N-vacancies in CN on perfluoroalkylation reactions.[176] They observed a significant increase in the adsorbent nature of N-vacancy CN when prepared at 620 °C under an argon atmosphere, in contrast to CN prepared under oxidative and reductive conditions. To explore the intriguing impact of N deficiency on photoredox reaction, the researchers conducted a comparison of the T_1/T_2 relaxation periods using ^{19}F NMR for their organofluorine-based substrates. The presence of N-containing moieties, resulting from defects in tri-s-triazine rings, heightened the interaction between perfluoroalkyl iodide, thereby playing a thermodynamically significant role by weakening the iodine-carbon bond in the reagent. Consequently, these newly created active sites in N-vacancy CN proved to be perfectly compatible for reactions such as perfluoroalkylation. To further enhance the impact of N-vacancy in CN on this reaction, the same research group increased the photocatalytic activity by prolonging the duration of the annealing process, aiming to make this method more practical for industrial applications.[164] This approach amplified the efficacy of the N-defect photocatalyst by a factor of six, outperforming the most recently documented up-to-the-minute N-vacancy CN in this category of reactions. Building upon this research, Xiao *et al.* investigated the perfluoroalkylation of alkynes employing N-vacancy CN.[177] They successfully achieved addition to and coupling with alkynes through a mechanism similar to the one employed in the earlier studies. A study has also documented the unfavorable aspects of the introduction of N vacancies in CN. An examination of the impact of N-defects in the reduction of nitroaromatic compounds has been reported.[25] To assess the difference between pristine and annealed CN, photoreduction performance and adsorption capacity were systematically tested using in situ XPS and post-mortem temperature-programmed desorption. In both analyses, hydrogen atoms exhibited a stronger binding affinity to the surface of N-defected CN compared to pristine CN. This stronger binding affinity (H_{ads}) was observed to hinder the conversion of nitrobenzene derivatives into the desired azo, azoxy, or aniline derivatives.

6. Challenges and Outlook

In contrast to traditional semiconducting metal oxides like TiO_2 and ZnO, CN has demonstrated a remarkable surge in research publications each year, establishing itself as a superior photocatalyst. This heightened interest has engendered a competitive atmosphere among researchers, fostering creativity in methodological approaches aimed at enhancing photocatalytic activity. The controlled manipulation of atomic vacancies within the CN structure represents a crucial avenue for tailoring its properties to meet specific applications. As the focus on N-vacancies within polymeric CN structures intensifies, future research is likely to probe deeper into refining synthesis strategies, characterizing defects with higher precision, and exploring novel applications.

***i)* Refinement of Synthesis Strategies**: Ongoing endeavors in the synthesis of N-vacancy CN via thermal treatment are likely to explore novel methodologies, optimizing parameters such as temperature, time, reaction atmosphere, etc. Alternative techniques such as rapid high-temperature treatments and thermal vacuum technologies may gain significance for efficiently inducing N-vacancies. However, researchers should prioritize controllable synthesis and parameters based on specific application requirements. For instance, only a limited number of studies have employed techniques like TGA/DSC to determine the optimum temperature for desired deficiencies. New methodologies, including those involving targeted N removal, are yet to be widely adopted, and the reproducibility of specific strategies and the product yield remains a critical consideration. A standardized language would prove highly beneficial for navigating through the existing literature on related studies. Terms such as N-vacancy, N-defect, amorphization, and imperfection describe a similar band engineering strategy in CN, yet pose a challenge during searches due to variations. Likewise, articulating the newly created energy levels (defect states, defect levels, intra-gap levels, etc.) at the band edges faces the same issue. Standardizing these terms would greatly enhance the clarity and coherence of literature in this field, addressing gaps and fostering a more comprehensive understanding.

***ii)* Advanced Characterization Techniques**: The advancements in advanced instrumental techniques for materials characterization have contributed to a more comprehensive understanding of defect types and their distribution in CN. The calculation of the C/N ratio is primarily carried out through methods such as XPS, energy-dispersive X-ray spectroscopy (EDX) or ssNMR. However, XPS and EDX predominantly measure surface composition and only a specific portion, respectively. On the other hand, the intensity of ssNMR is influenced by the surrounding hydrogen atoms in the structure. Consequently, there arises a need for a novel approach to determine the composition of defects in CN. Furthermore, in certain investigations, satellite peaks in ^{13}C CP MAS NMR are mistakenly identified as cyano group peaks due to unattained anisotropy. The inclusion of PAS and X-ray absorption spectroscopy (XAS), along with related techniques like resonant inelastic X-ray scattering and operando instruments, is crucial to enhance the elucidation of specific defects.[178] Up to now, XAS has predominantly been employed to investigate cases where a heteroatom, mostly a metal, is doped into CN.[179–182] These advanced techniques enable a more comprehensive understanding of structural alterations in CN, encompassing changes in bond lengths, strengths, and the chemical environment.[183]

© 2024 The Authors. ChemCatChem published by Wiley-VCH GmbH

18673899, 0, Downloaded from https://chemistry-europe.onlinelibrary.wiley.com/doi/10.1002/cctc.202301560 by Koc University, Wiley Online Library on [12/07/2024]. See the Terms and Conditions (https://onlinelibrary.wiley.com/terms-and-conditions) on Wiley Online Library for rules of use; OA articles are governed by the applicable Creative Commons License

However, it's worth noting that this approach is currently underutilized in the context of N-vacancy CN, indicating a significant gap in our knowledge of this specific aspect.[184,185] Moreover, Data analysis and interpretation, however, still exhibit contradictions independent of the synthesis method and additives used. While many studies support their experimental results with DFT, the calculated energy required for the removal of N_{2C}/N_{3C} or NH_x varies between studies. However, experimental results in most of the studies revealed the opposite. Moreover, despite the observation of the Urbach tail in absorbance spectroscopy, the majority of studies have been eager to comprehensively investigate these advantageous optical properties. There is also a shortage of studies exploring and validating the increased adsorption capacity of N-deficient CN, despite its known efficacy in photooxidation reactions and O_2 molecules.

iii) **Application Exploration**: Additional exploration of the application potential of N-vacancy CN is anticipated, not only in photocatalysis but also in fields such as optoelectronics, sensing, and energy storage. Investigations into the influence of defects on the electronic and optical properties of CN may unveil opportunities for designing new materials with tailored functionalities. While the introduction of N-vacancies predominantly narrows the bandgap and enhanced photocatalytic performance, the aforementioned studies reporting photoredox transformations with suboptimal results should be improved for standardization. Researchers should contemplate a tunable bandgap with high redox abilities achievable through specific methodologies. The demand for an ideal photocatalyst with multifunctionality, addressing more than one application, remains unfulfilled.

iv) **Multi-Doping or Heterojunction Strategies**: Subsequent studies may explore the synergistic effects of introducing N-vacancies alongside non-elemental dopants to enhance specific material properties or enable new functionalities. Upon evaluating the Fermi level of the resultant N-vacancy in CN, it can be strategically coupled with a compatible semiconductor to establish a heterojunction. This deliberate combination aims to enhance the redox capability, leveraging the distinctive features of the N-deficient CN.

;***v)*** **N-vacancy-photocatalytic activity mechanism**: The current literature lacks mechanistic studies correlating the structure-activity relationship concerning N-vacancies. Additionally, the creation of active sites through N-deficiency and their role in the photocatalytic mechanism should be clarified. The precise role of midgap states in the electron transfer process is currently a topic of ongoing debate. Consequently, unraveling the optimal position of midgap states and elucidating their specific role will significantly enhance the depth of mechanism studies during the photocatalytic process.

7. Conclusions

In conclusion, this review highlights the profound impact of N-vacancies in polymeric CN structures on material behavior. The comprehensive analysis of these defects, facilitated by advanced characterization techniques, has advanced our understanding of their potential across various photocatalytic applications. Synthesis strategies, particularly thermal treatments, have proven effective in inducing N-vacancies and tailoring the photophysical properties and photocatalytic performance of CN. Researchers' intense interest in exploring diverse fields, from photocatalysis to optoelectronics, points to a promising trajectory for this field due to the advanced features provided by these vacancies. Looking ahead, continued growth is anticipated, with a focus on refining synthesis techniques, uncovering new applications, and gaining deeper insights into the intricate relationships between N-vacancies and material properties. The researchers have dedicated significant efforts to optimizing the N-vacancy content in CN and understanding the structure-activity relationship, particularly in certain model reactions. While these studies have predominantly focused on photooxidation reactions, ranging from photodegradation to H_2O_2 production, there remains a gap in addressing the selective oxidation of organic molecules beyond benzyl alcohol derivatives. Moreover, nitrogen fixation has been explored to a limited extent compared to other chemical transformations. To address these gaps, we strongly recommend exploring nitrogen reduction, utilizing the resulting NH_3 as a nucleophile for the amination of aromatic compounds or the production of imine/amine derivatives. Such tandem reactions not only promise eco-friendly and sustainable practices but also hold significant practical potential. Additionally, it is noteworthy that the chemical stability and visible light harvesting ability of N-vacancy CN tend to decrease after 5 cycles. To facilitate catalyst reuse, we propose considering an upcycling strategy that allows for the regeneration of the catalyst without altering the defect/active sites within the structure. The multifaceted approach to defect engineering in CN not only enhances our understanding of this unique material but also reveals new possibilities for designing advanced materials with tailored functionalities for a diverse range of technological applications. The integration of sustainable practices and the optimization of catalyst stability will undoubtedly contribute to the development of efficient and environmentally conscious solutions in the field of catalysis.

Acknowledgements

The authors thank to Turkish Academy of Sciences (TUBA) for the financial support. All authors thank to Ayman Batuhan Ayyıldız for his outstanding effort and creativity in crafting the graphical abstract for this review article.

Conflict of Interests

The authors declare no conflict of interest.

Keywords: Graphitic carbon nitride · N-vacancy · Midgap states · Point defect engineering · Photocatalysis

© 2024 The Authors. ChemCatChem published by Wiley-VCH GmbH

[1] A. K. Geim, K. S. Novoselov, *Nat. Mater.* **2007**, *6*, 183.
[2] O. Savateev, M. Antonietti, X. Wang, *Carbon nitrides: Structure, properties and applications in science and technology*, De Gruyter, **2023**, pp. 2–40.
[3] A. Thomas, A. Fischer, F. Goettmann, M. Antonietti, J. O. Müller, R. Schlögl, J. M. Carlsson, *J. Mater. Chem.* **2008**, *18*, 4893.
[4] X. Wang, K. Maeda, A. Thomas, K. Takanabe, G. Xin, J. M. Carlsson, K. Domen, M. Antonietti, *Nat. Mater.* **2009**, *8*, 76.
[5] W.-J. Ong, L.-L. Tan, Y. H. Ng, S.-T. Yong, S.-P. Chai, *Chem. Rev.* **2016**, *116*, 7159.
[6] X. Yu, S. F. Ng, L. K. Putri, L. L. Tan, A. R. Mohamed, W. J. Ong, *Small* **2021**, *17*, 2006851.
[7] R. Huang, J. Wu, M. Zhang, B. Liu, Z. Zheng, D. Luo, *Mater. Des.* **2021**, *210*, 110040.
[8] L. Jiang, J. Yang, S. Zhou, H. Yu, J. Liang, W. Chu, H. Li, H. Wang, Z. Wu, X. Yuan, *Coord. Chem. Rev.* **2021**, *439*, 213947.
[9] S. J. Mun, S. J. Park, *Catalysts* **2019**, *9*, 805.
[10] K. A. Adegoke, N. W. Maxakato, *Mater. Today Chem.* **2022**, *23*, 100605.
[11] N. Rono, J. K. Kibet, B. S. Martincigh, V. O. Nyamori, *A review of the current status of graphitic carbon nitride*, Vol. 46, Taylor & Francis, **2021**, pp. 189–217.
[12] W. K. Darkwah, Y. Ao, *Nanoscale Res. Lett.* **2018**, *13*, 1.
[13] B. Tian, D. Ho, J. Qin, J. Hu, Z. Chen, D. Voiry, Q. Wang, Z. Zeng, *Prog. Mater. Sci.* **2023**, *133*, 101056.
[14] G. Z. S. Ling, V. B. Y. Oh, C. Y. Haw, L. L. Tan, W. J. Ong, *Energy Mater. Adv.* **2023**, *4*.
[15] C. Tang, M. Cheng, C. Lai, L. Li, X. Yang, L. Du, G. Zhang, G. Wang, L. Yang, *Coord. Chem. Rev.* **2023**, *474*, 214846.
[16] Y. Sun, V. Kumar, K. H. Kim, *Sep. Purif. Technol.* **2023**, *305*, 122413.
[17] H. Starukh, P. Praus, *Catalysts* **2020**, *10*, 1.
[18] G. Liao, C. Li, X. Li, B. Fang, *Cell Reports Phys. Sci.* **2021**, *2*, 100355.
[19] J. Li, K. Huang, Y. Huang, Y. Ye, M. Ziółek, Z. Wang, S. Yue, M. Ma, J. Liu, K. Liu, S. Qu, Z. Zhao, Y. Zhang, Z. Wang, *J. Semicond.* **2023**, *44*, 081701.
[20] Y. Li, Z. He, L. Liu, Y. Jiang, W. J. Ong, Y. Duan, W. Ho, F. Dong, *Nano Energy* **2023**, *105*, 108032.
[21] A. Kumar, P. Raizada, A. Hosseini-Bandegharaei, V. K. Thakur, V. H. Nguyen, P. Singh, *J. Mater. Chem. A* **2021**, *9*, 111.
[22] J. Tan, N. Tian, Z. Li, J. Li, X. Yao, M. Vakili, Y. Lu, T. Zhang, *Chem. Eng. J.* **2021**, *421*, 127729.
[23] X. Chen, L. Liu, P. Y. Yu, S. S. Mao, *Science* **2011**, *331*, 746.
[24] W. Tu, Y. Xu, J. Wang, B. Zhang, T. Zhou, S. Yin, S. Wu, C. Li, Y. Huang, Y. Zhou, Z. Zou, J. Robertson, M. Kraft, R. Xu, *ACS Sustainable Chem. Eng.* **2017**, *5*, 7260.
[25] Y. Dai, C. Li, Y. Shen, T. Lim, J. Xu, Y. Li, H. Niemantsverdriet, F. Besenbacher, N. Lock, R. Su, *Nat. Commun. 2017 91* **2018**, *9*, 1.
[26] X. Chu, C. I. Sathish, J. H. Yang, X. Guan, X. Zhang, L. Qiao, K. Domen, S. Wang, A. Vinu, J. Yi, *Small* **2023**, *19*, 2302875.
[27] J. Xue, M. Fujitsuka, T. Majima, *ACS Appl. Mater. Interfaces* **2019**, *11*, 40860.
[28] R. tang Guo, J. Wang, Z. xu Bi, X. Chen, X. Hu, W. guo Pan, *Chemosphere* **2022**, *295*, 133834.
[29] Y. Zhang, J. Yuan, Y. Ding, B. Liu, L. Zhao, S. Zhang, *Ceram. Int.* **2021**, *47*, 31005.
[30] S. Hou, X. Gao, S. Wang, X. Yu, J. Liao, D. Su, *Small* **2023**, *19*, 2302500.
[31] F. K. Kessler, Y. Zheng, D. Schwarz, C. Merschjann, W. Schnick, X. Wang, M. J. Bojdys, *Nat. Rev. Mater.* **2017**, *2*, 1.
[32] J. Safaei, N. A. Mohamed, M. F. Mohamad Noh, M. F. Soh, N. A. Ludin, M. A. Ibrahim, W. N. Roslam Wan Isahak, M. A. Mat Teridi, *J. Mater. Chem. A* **2018**, *6*, 22346.
[33] X. Zhang, M. Li, W. Han, S. E. Wu, H. Wang, S. Liu, Z. Tang, L. Zeng, *Mater. Des.* **2023**, *235*, 112405.
[34] H. Y. Hoh, Y. Zhang, Y. L. Zhong, Q. Bao, *Adv. Opt. Mater.* **2021**, *9*, 2100146.
[35] M. M. Xavier, P. R. Nair, S. Mathew, *Analyst* **2019**, *144*, 1475.
[36] Z. Zhou, Y. Zhang, Y. Shen, S. Liu, Y. Zhang, *Chem. Soc. Rev.* **2018**, *47*, 2298.
[37] H. Liu, S. Ma, L. Shao, H. Liu, Q. Gao, B. Li, H. Fu, S. Fu, H. Ye, F. Zhao, J. Zhou, *Appl. Catal. B* **2020**, *261*, 118201.
[38] X. Xu, Y. Xu, Y. Liang, H. Long, D. Chen, H. Hu, J. Z. Ou, *Mater. Chem. Front.* **2022**, *6*, 3143.
[39] M. Tahir, A. Sherryna, A. A. Khan, M. Madi, A. Y. Zerga, B. Tahir, *Energy and Fuels* **2022**, *36*, 8948.
[40] S. Bai, N. Zhang, C. Gao, Y. Xiong, *Nano Energy* **2018**, *53*, 296.
[41] E. G. Seebauer, K. W. Noh, *Mater. Sci. Eng. R* **2010**, *70*, 151.
[42] X. Yan, L. Zhuang, Z. Zhu, X. Yao, *Nanoscale* **2021**, *13*, 3327.
[43] J. Xiong, J. Di, J. Xia, W. Zhu, H. Li, J. Xiong, J. Di, J. Xia, W. Zhu, H. Li, *Adv. Funct. Mater.* **2018**, *28*, 1801983.
[44] Q. Lai, H. Zheng, Z. Tang, D. Bi, N. Chen, X. Liu, J. Zheng, Y. Liang, *ACS Appl. Mater. Interfaces* **2021**, *13*, 61129.
[45] B. Gao, M. Dou, J. Wang, S. Li, D. Wang, L. Ci, Y. Fu, *Chem. Eng. J.* **2021**, *426*, 131677.
[46] P. Niu, G. Liu, H. M. Cheng, *J. Phys. Chem. C* **2012**, *116*, 11013.
[47] Z. Li, G. Gu, S. Hu, X. Zou, G. Wu, *Chin. J. Catal.* **2019**, *40*, 1178.
[48] Y. Zheng, Y. Luo, Q. Ruan, J. Yu, X. Guo, W. Zhang, H. Xie, Z. Zhang, J. Zhao, Y. Huang, *J. Colloid Interface Sci.* **2022**, *609*, 75.
[49] X. Qu, S. Hu, P. Li, Z. Li, H. Wang, H. Ma, W. Li, *Diamond Relat. Mater.* **2018**, *86*, 159.
[50] X. Li, J. Zhang, F. Zhou, H. Zhang, J. Bai, Y. Wang, H. Wang, *Cuihua Xuebao/Chinese J. Catal.* **2018**, *39*, 1090.
[51] D. Wang, X. Gu, G. Liu, G. Huang, Y. Cao, Y. Guo, *Int. J. Hydrogen Energy* **2021**, *46*, 5158.
[52] X. Wang, L. Wu, Z. Wang, H. Wu, X. Zhou, H. Ma, H. Zhong, Z. Xing, G. Cai, C. Jiang, F. Ren, *Solar RRL* **2019**, *3*, 1800298.
[53] Y. Liu, X. Guo, Z. Chen, W. Zhang, Y. X. Wang, Y. Zheng, X. Tang, M. Zhang, Z. Peng, R. Li, Y. Huang, *Appl. Catal. B* **2020**, *266*, 118624.
[54] J. S. Kim, J. W. Oh, S. I. Woo, *Catal. Today* **2017**, *293–294*, 8.
[55] F. Dong, Z. Wang, Y. Sun, W. K. Ho, H. Zhang, *J. Colloid Interface Sci.* **2013**, *401*, 70.
[56] Y. Hou, J. Yang, C. Lei, B. Yang, Z. Li, Y. Xie, X. Zhang, L. Lei, J. Chen, *ACS Sustainable Chem. Eng.* **2018**, *6*, 6497.
[57] L. Liang, L. Shi, F. Wang, *Diamond Relat. Mater.* **2019**, *91*, 230.
[58] S. Hu, D. Jiang, L. Gu, G. Xu, Z. Li, Y. Yuan, *Chem. Eng. J.* **2020**, *399*, 125847.
[59] T. Kubanaliev, Z. Eroglu, M. S. Ozer, Ö. Metin, *Catal. Sci. Technol.* **2023**, *13*, 2317.
[60] A. Ghosh, H. Saini, A. Sarkar, P. Guha, A. K. Samantara, R. Thapa, S. Mandal, A. Mandal, J. N. Behera, S. K. Ray, D. K. Goswami, *Appl. Surf. Sci.* **2021**, *556*, 149773.
[61] F. Yang, H. Li, K. Pan, S. Wang, H. Sun, Y. Xie, Y. Xu, J. Wu, W. Zhou, *Solar RRL* **2021**, *5*, 2000610.
[62] J. Zhang, J. Chen, Y. Wan, H. Liu, W. Chen, G. Wang, R. Wang, *ACS Appl. Mater. Interfaces* **2020**, *12*, 13805.
[63] Y. Zhang, Z. Huang, C. L. Dong, J. Shi, C. Cheng, X. Guan, S. Zong, B. Luo, Z. Cheng, D. Wei, Y. cheng Huang, S. Shen, L. Guo, *Chem. Eng. J.* **2022**, *431*, 134101.
[64] F. Lin, T. Wang, Z. Ren, X. Cai, Y. Wang, J. Chen, J. Wang, S. Zang, F. Mao, L. Lv, *J. Colloid Interface Sci.* **2023**, *636*, 223.
[65] Q. Li, Y. Jiao, Y. Tang, J. Zhou, B. Wu, B. Jiang, H. Fu, *J. Am. Chem. Soc.* **2023**, *145*.
[66] L. Kong, X. Mu, X. Fan, R. Li, Y. Zhang, P. Song, F. Ma, M. Sun, *Appl. Mater. Today* **2018**, *13*, 329.
[67] J. Fu, Z. Mo, H. Chen, Z. Chen, X. Zhu, J. Yan, J. Liu, Y. Wei, H. Li, H. Xu, *J. Environ. Chem. Eng.* **2023**, *11*, 109495.
[68] H. Zhang, Y. Zhu, Y. Sun, J. Khan, H. Liu, J. Xiao, H. Zhou, L. Han, *J. Environ. Chem. Eng.* **2023**, *11*, 111122.
[69] V. Hasija, P. Singh, S. Thakur, V. H. Nguyen, Q. Van Le, T. Ahamad, S. M. Alshehri, P. Raizada, B. M. Matsagar, K. C. W. Wu, *Chemosphere* **2023**, *320*, 138015.
[70] H. Zhai, P. Tan, L. Lu, H. Liu, Y. Liu, J. Pan, *Catal. Sci. Technol.* **2021**, *11*, 3914.
[71] Y. Liao, G. Wang, J. Wang, K. Wang, S. Yan, Y. Su, *J. Colloid Interface Sci.* **2021**, *587*, 110.
[72] C. N. R. Rao, K. Biswas, *Annu. Rev. Anal. Chem.* **2009**, *2*, 435.
[73] B. V. Lotsch, M. Döblinger, J. Sehnert, L. Seyfarth, J. Senker, O. Oeckler, W. Schnick, *Chem. A Eur. J.* **2007**, *13*, 4969.
[74] Y. Zhang, J. Liu, G. Wu, W. Chen, *Nanoscale* **2012**, *4*, 5300.
[75] Q. Zhang, L. Li, Q. Zhou, H. H. Zhang, H. H. Zhang, B. An, H. Ning, T. Xing, M. Wang, M. Wu, W. Wu, *ACS Catal.* **2023**, *13*, 13101.
[76] X. Li, C. Zhang, C. Xiong, L. Kong, M. Yu, X. Fan, *J. Build. Eng.* **2023**, *70*, 106259.
[77] H. Lan, Q. Tang, Z. Hou, K. Zhu, X. An, H. Liu, J. Qu, *ACS ES T Eng.* **2023**, *3*, 580.
[78] X. Liu, X. Pan, Y. Qiu, J. Li, X. Ma, D. Li, *Langmuir* **2023**, *39*, 11294.
[79] T. K. A. Nguyen, T. T. Pham, B. Gendensuren, E. S. Oh, E. W. Shin, *J. Mater. Sci. Technol.* **2022**, *103*, 232.
[80] N. Sun, Y. Liang, X. Ma, F. Chen, *Chem. A Eur. J.* **2017**, *23*, 15466.
[81] H. Shi, S. Long, J. Hou, L. Ye, Y. Sun, W. Ni, C. Song, K. Li, G. G. Gurzadyan, X. Guo, *Chem. A Eur. J.* **2019**, *25*, 5028.

© 2024 The Authors. ChemCatChem published by Wiley-VCH GmbH

18673899, 0, Downloaded from https://chemistry-europe.onlinelibrary.wiley.com/doi/10.1002/cctc.202301560 by Koc University, Wiley Online Library on [12/07/2024]. See the Terms and Conditions (https://onlinelibrary.wiley.com/terms-and-conditions) on Wiley Online Library for rules of use; OA articles are governed by the applicable Creative Commons License

[82] X. Chen, B. Chu, Q. Gu, H. Liu, C. Li, W. Li, J. Lu, D. Wu, *J. Environ. Chem. Eng.* **2021**, *9*, 106380.
[83] J. Huang, Y. Cao, H. Wang, H. Yu, F. Peng, H. Zou, Z. Liu, *Chem. Eng. J.* **2019**, *373*, 687.
[84] A. Gupta, T. Bhoyar, B. M. Abraham, D. J. Kim, K. S. Pasupuleti, S. S. Umare, D. Vidyasagar, A. Gedanken, *ACS Appl. Mater. Interfaces* **2023**, *15*, 18898.
[85] S. Li, W. Si, L. Cui, L. Shi, *Diamond Relat. Mater.* **2020**, *110*, 108149.
[86] W. Yu, X. Shan, Z. Zhao, *Appl. Catal. B* **2020**, *269*, 118778.
[87] F. Liu, Z. Yao, S. Xu, X. Fan, X. Zhang, J. Yuan, Y. Yu, X. Zhu, Z. Xiong, H. Yu, *J. Mater. Sci. Mater. Electron.* **2022**, *33*, 14535.
[88] X. Zhan, Y. Zeng, H. Zhang, X. Wang, D. Jin, H. Jin, S. Luo, L. Yang, B. Hong, *J. Environ. Chem. Eng.* **2023**, *11*, 109201.
[89] Y. Liu, L. Zhao, X. Zeng, F. Xiao, W. Fang, X. Du, X. He, D. Wang, W. Li, H. Chen, *Mater. Today Energy* **2023**, *31*, 101211.
[90] C. Fernández-Ramos, M. J. Sayagués, T. C. Rojas, M. D. Alcalá, C. Real, A. Fernández, *Diamond Relat. Mater.* **2000**, *9*, 212.
[91] M. Liu, J. Liu, Z. Zeng, X. Wang, J. Jia, X. Gu, Z. Zheng, *Sep. Purif. Technol.* **2022**, *300*, 121929.
[92] Y. Zhang, J. Gao, Z. Chen, *J. Colloid Interface Sci.* **2019**, *535*, 331.
[93] Q. Han, B. Wang, J. Gao, Z. Cheng, Y. Zhao, Z. Zhang, L. Qu, *ACS Nano* **2016**, *10*, 2745.
[94] J. Xue, M. Fujitsuka, T. Majima, *Phys. Chem. Chem. Phys.* **2019**, *21*, 2318.
[95] Y. Cong, S. Zhang, Q. Zheng, X. Li, Y. Zhang, S. W. Lv, *J. Colloid Interface Sci.* **2023**, *650*, 1013.
[96] C. Liu, W. Ma, J. Chen, Z. Mao, D. Wang, *J. Mater. Sci. Mater. Electron.* **2021**, *32*, 25033.
[97] Y. Liu, W. Yin, Q. Lin, Z. Li, W. Zhong, B. Fang, *Appl. Surf. Sci.* **2023**, *640*, 158386.
[98] H. Yu, R. Shi, Y. Y. Zhao, T. Bian, Y. Y. Zhao, C. Zhou, G. I. N. Waterhouse, L.-Z. L. Wu, C.-H. C. Tung, T. Zhang, H. Yu, R. Shi, Y. Y. Zhao, T. Bian, C. Zhao, L.-Z. L. Wu, C.-H. C. Tung, T. Zhang, G. I. N. Waterhouse, *Adv. Mater.* **2017**, *29*, 1605148.
[99] X. Zhang, G. Yang, J. Meng, L. Qin, M. Ren, Y. Pan, Y. Yang, Y. Guo, *Small* **2023**, *19*, 2208012.
[100] Q. Li, Y. Tong, Y. Zeng, X. K. Gu, M. Ding, *Chem. Eng. J.* **2022**, *450*, 138010.
[101] J. Liao, W. Cui, J. Li, J. Sheng, H. Wang, X. Dong, P. Chen, G. Jiang, Z. Wang, F. Dong, *Chem. Eng. J.* **2020**, *379*, 122282.
[102] X. Yang, X. Wang, J. Yang, X. Bian, X. Yu, X. Huo, Q. Qi, R. Jia, *New J. Chem.* **2022**, *46*, 13783.
[103] Q. Zhang, Y. Sun, J. Deng, Y. Liu, Y. H. Ng, L. Jing, H. Dai, *Int. J. Hydrogen Energy* **2023**, *48*, 31590.
[104] J. Shen, C. Luo, S. Qiao, Y. Chen, Y. Tang, J. Xu, K. Fu, D. Yuan, H. Tang, H. Zhang, C. Liu, *ACS Catal.* **2023**, *13*, 6280.
[105] V. Hasija, P. Singh, S. Thakur, V.-H. Nguyen, Q. Van Le, T. Ahamad, S. M. Alshehri, P. Raizada, B. Matsagar, K. C.-W. Wu, *SSRN Electron. J.* **2022**, DOI 10.2139/SSRN.4255557.
[106] Y. J. Lee, Y. J. Jeong, I. S. Cho, S. J. Park, C. G. Lee, P. J. J. Alvarez, *J. Hazard. Mater.* **2023**, *449*, 131046.
[107] Q. Si, H. Wang, J. Kuang, B. Liu, S. Zheng, Q. Zhao, W. Jia, Y. Wu, H. Lu, Q. Wu, T. Yu, W. Guo, *J. Hazard. Mater.* **2023**, *454*, 131463.
[108] Y. Shiraishi, S. Shiota, Y. Kofuji, M. Hashimoto, K. Chishiro, H. Hirakawa, S. Tanaka, S. Ichikawa, T. Hirai, *ACS Appl. Energ. Mater.* **2018**, *1*, 4169.
[109] J. Lei, B. Chen, W. Lv, L. Zhou, L. Wang, Y. Liu, J. Zhang, *ACS Sustainable Chem. Eng.* **2019**, *7*, 16467.
[110] L. L. Liu, F. Chen, J. H. Wu, M. K. Ke, C. Cui, J. J. Chen, H. Q. Yu, *Appl. Catal. B* **2022**, *302*, 120845.
[111] X. Zhang, P. Ma, C. Wang, L. Gan, X. Chen, P. Zhang, Y. Wang, H. Li, L. Wang, X. Zhou, K. Zheng, *Energy Environ. Sci.* **2022**, *15*, 830.
[112] C. Zhao, C. Shi, Q. Li, X. Wang, G. Zeng, S. Ye, B. Jiang, J. Liu, *Mater. Today Energy* **2022**, *24*, 100926.
[113] A. Actis, M. Melchionna, G. Filippini, P. Fornasiero, M. Prato, E. Salvadori, M. Chiesa, *Angew. Chem. Int. Ed.* **2022**, *61*, e202210640.
[114] A. Actis, P. Fornasiero, M. Chiesa, E. Salvadori, M. A. Actis, *ChemPhotoChem* **2023**, *7*, e202300203.
[115] J. Coates, *Encycl. Anal. Chem.* **2000**, DOI 10.1002/9780470027318.A5606.
[116] X. Zhao, Q. Liu, X. Li, H. Li, Z. Shen, H. Ji, T. Ma, *Angew. Chem. Int. Ed.* **2023**, *62*, e202219214.
[117] M. R. Gholipour, F. Béland, T. O. Do, *ACS Sustainable Chem. Eng.* **2017**, *5*, 213.
[118] Z. Wang, Y. Huang, M. Chen, X. Shi, Y. Zhang, J. Cao, W. Ho, S. C. Lee, *ACS Appl. Mater. Interfaces* **2019**, *11*, 10651.
[119] C. Fu, M. Zhao, X. Chen, G. Sun, C. Wang, Q. Song, *Appl. Catal. B* **2023**, *332*, 122752.
[120] H. Li, C. Jin, Z. Wang, Y. Liu, P. Wang, Z. Zheng, M. H. Whangbo, L. Kou, Y. Li, Y. Dai, B. Huang, *Chem. Eng. J.* **2019**, *369*, 263.
[121] Y. Zheng, Y. Luo, Q. Ruan, S. Wang, J. Yu, X. Guo, W. Zhang, H. Xie, Z. Zhang, Y. Huang, *Appl. Catal. B* **2022**, *311*, 121372.
[122] B. Reif, S. E. Ashbrook, L. Emsley, M. Hong, *Nat. Rev. Methods Prim.* **2021**, *1*, 1.
[123] S. Li, O. Lafon, W. Wang, Q. Wang, X. Wang, Y. Li, J. Xu, F. Deng, *Adv. Mater.* **2020**, *32*, 2002879.
[124] J. J. Fitzgerald, S. M. DePaul, *ACS Symp. Ser.* **1999**, *717*, 2.
[125] B. Jürgens, E. Irran, J. Senker, P. Kroll, H. Müller, W. Schnick, *J. Am. Chem. Soc.* **2003**, *125*, 10288.
[126] J. Sun, B. Zhang, W. Chen, Z. Tao, J. Liu, L. Wang, *Carbon* **2023**, *209*, 117988.
[127] Q. Guo, Y. Wu, L. Xia, X. F. Yu, K. Zhang, Y. Du, L. Zhang, H. Tang, J. Cheng, J. Shang, Y. Peng, Z. Li, X. Man, X. Yang, *Chem. Eng. J.* **2023**, *452*, 139092.
[128] D. Wang, Z. Zhang, S. Xu, Y. Guo, S. Kang, X. Chang, *Int. J. Mol. Sci.* **2022**, *23*, 7381.
[129] M. Razavi-Esfali, T. Mahvelati-Shamsabadi, H. Fattahimoghaddam, B. K. Lee, *Chem. Eng. J.* **2021**, *419*, 129503.
[130] Y. Hu, Y. Shim, J. Oh, S. Park, S. Park, Y. Ishii, *Chem. Mater.* **2017**, *29*, 5080.
[131] H. Sun, F. Guo, J. Pan, W. Huang, K. Wang, W. Shi, *Chem. Eng. J.* **2021**, *406*, 126844.
[132] M. Yang, R. Duan, J. Mei, B. Yang, H. Yang, S. Sun, S. Liang, J. Cui, *Int. J. Hydrogen Energy* **2023**, *48*, 9690.
[133] P. Deng, Y. Liu, L. Shi, L. Cui, W. Si, L. Yao, *Opt. Mater.* **2021**, *120*, 111407.
[134] Y. Huang, J. Liu, C. Zhao, X. Jia, M. Ma, Y. Qian, C. Yang, K. Liu, F. Tan, Z. Z. Wang, X. Li, S. Qu, Z. Z. Wang, *ACS Appl. Mater. Interfaces* **2020**, *12*, 52603.
[135] X. Zhang, Y. Liu, M. Ren, G. Yang, L. Qin, Y. Guo, J. Meng, *Chem. Eng. J.* **2022**, *433*, 134551.
[136] F. He, S. Cheng, H. Song, C. Zhao, J. Zhang, S. Wang, H. Sun, *Langmuir* **2022**, *38*, 828.
[137] J. He, N. Li, Z. G. Li, M. Zhong, Z. X. Fu, M. Liu, J. C. Yin, Z. Shen, W. Li, J. Zhang, Z. Chang, X. H. Bu, *Adv. Funct. Mater.* **2021**, *31*, 2103597.
[138] M. Cao, S. Shao, W. Wei, J. B. Love, Z. Yue, Y. Zhang, X. Zhang, Y. Xue, J. Yu, X. Fan, *Appl. Surf. Sci.* **2024**, *643*, 158653.
[139] S. Wang, X. Wang, B. Liu, X. Xiao, L. Wang, W. Huang, *J. Colloid Interface Sci.* **2022**, *610*, 495.
[140] C. Cheng, J. Shi, L. Wen, C. L. Dong, Y. C. Huang, Y. Zhang, S. Zong, Z. Diao, S. Shen, L. Guo, *Carbon* **2021**, *181*, 193.
[141] F. Tuomisto, I. Makkonen, *Rev. Mod. Phys.* **2013**, *85*, 1583.
[142] F. A. Selim, *Mater. Charact.* **2021**, *174*, 110952.
[143] P. Praus, L. Řeháčková, J. Čížek, A. Smýkalová, M. Koštejn, J. Pavlovský, M. Filip Edelmannová, K. Kočí, *Sci. Reports* **2022**, *12*, 1.
[144] X. Wang, S. Blechert, M. Antonietti, *ACS Catal.* **2012**, *2*, 1596.
[145] Y. Wang, X. Wang, M. Antonietti, *Angew. Chem. Int. Ed.* **2012**, *51*, 68.
[146] Y. Zheng, J. Liu, J. Liang, M. Jaroniec, S. Z. Qiao, *Energy Environ. Sci.* **2012**, *5*, 6717.
[147] E. Kroke, M. Schwarz, E. Horath-Bordon, P. Kroll, B. Noll, A. D. Norman, *New J. Chem.* **2002**, *26*, 508.
[148] B. Zhu, B. Cheng, L. Zhang, J. Yu, *Carbon Energy* **2019**, *1*, 32.
[149] B. Zhu, L. Zhang, B. Cheng, J. Yu, *Appl. Catal. B* **2018**, *224*, 983.
[150] H. Z. Wu, L. M. Liu, S. J. Zhao, *Appl. Surf. Sci.* **2015**, *358*, 363.
[151] E. Raciti, S. M. Gali, M. Melchionna, G. Filippini, A. Actis, M. Chiesa, M. Bevilacqua, P. Fornasiero, M. Prato, D. Beljonne, R. Lazzaroni, *Chem. Sci.* **2022**, *13*, 9927.
[152] H. Tan, P. Kong, R. Zhang, M. Gao, M. Liu, X. Gu, W. Liu, Z. Zheng, *Innovation* **2021**, *2*, 100089.
[153] A. Ghosh, H. Saini, A. Sarkar, P. Guha, A. K. Samantara, R. Thapa, S. Mandal, A. Mandal, J. N. Behera, S. K. Ray, D. K. Goswami, *Appl. Surf. Sci.* **2021**, *556*, 149773.
[154] X. Liu, W. Kang, W. Zeng, Y. Zhang, L. Qi, F. Ling, L. Fang, Q. Chen, M. Zhou, *Appl. Surf. Sci.* **2020**, *499*, 143994.
[155] M. Wang, C. Fan, S. Yang, M. Liu, J. Luo, Y. Liu, L. Tang, Z. Gong, S. Leng, *Catal. Sci. Technol.* **2020**, *10*, 6800.
[156] P. Song, S. Sun, J. Cui, X. Zheng, S. Liang, *Appl. Surf. Sci.* **2021**, *568*, 150986.
[157] D. M. Schultz, T. P. Yoon, *Science* **2014**, *343*.
[158] H. Kisch, *Angew. Chem. Int. Ed.* **2013**, *52*, 812.
[159] N. Serpone, A. V. Emeline, *J. Phys. Chem. Lett.* **2012**, *3*, 673.

© 2024 The Authors. ChemCatChem published by Wiley-VCH GmbH

18673899, 0, Downloaded from https://chemistry-europe.onlinelibrary.wiley.com/doi/10.1002/cctc.202301560 by Koc University, Wiley Online Library on [12/07/2024]. See the Terms and Conditions (https://onlinelibrary.wiley.com/terms-and-conditions) on Wiley Online Library for rules of use; OA articles are governed by the applicable Creative Commons License

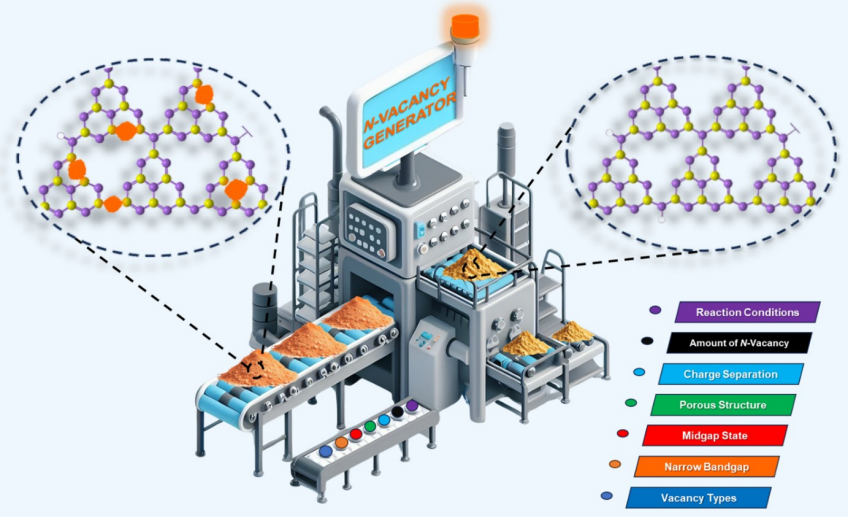
[160] M. Fagnoni, *Angew. Chem. Int. Ed.* **2010**, *49*, 6709.
[161] A. B. Djurišić, Y. He, A. M. C. Ng, *APL Mater.* **2020**, *8*, 30903.
[162] A. Actis, M. Melchionna, G. Filippini, P. Fornasiero, M. Prato, M. Chiesa, E. Salvadori, *Angew. Chem. Int. Ed.* **2023**, *62*, e202313540.
[163] H. Lin, J. Wu, F. Zhou, X. Zhao, P. Lu, G. Sun, Y. Song, Y. Li, X. Liu, H. Dai, *J. Environ. Sci.* **2023**, *124*, 570.
[164] F. Longobardo, G. Gentile, A. Criado, A. Actis, S. Colussi, V. Dal Santo, M. Chiesa, G. Filippini, P. Fornasiero, M. Prato, M. Melchionna, *Mater. Chem. Front.* **2021**, *5*, 7267.
[165] F. Li, X. Yue, D. Zhang, J. Fan, Q. Xiang, *Appl. Catal. B* **2021**, *292*, 120179.
[166] F. Urbach, *Phys. Rev.* **1953**, *92*, 1324.
[167] J. Y. Tang, X. Y. Kong, B. J. Ng, Y. H. Chew, A. R. Mohamed, S. P. Chai, *Catal. Sci. Technol.* **2019**, *9*, 2335.
[168] Q. Huang, Y. Liu, W. Bai, J. Hong, Y. Ai, Z. Chen, *Environ. Sci.-Nano* **2022**, *365*, 4445.
[169] Y. Shao, X. Hao, S. Lu, Z. Jin, *Chem. Eng. J.* **2023**, *454*, 140123.
[170] Y. Xie, Y. Li, Z. Huang, J. Zhang, X. Jia, X. S. Wang, J. Ye, *Appl. Catal. B* **2020**, *265*, 118581.
[171] Y. Shiraishi, Y. Kofuji, H. Sakamoto, S. Tanaka, S. Ichikawa, T. Hirai, *ACS Catal.* **2015**, *5*, 3058.
[172] J. Luo, Y. Liu, C. Fan, L. Tang, S. Yang, M. Liu, M. Wang, C. Feng, X. Ouyang, L. Wang, L. Xu, J. Wang, M. Yan, *ACS Catal.* **2021**, *11*, 11440.
[173] J. Li, J. Huang, G. Zeng, C. Zhang, H. Yu, Q. Wan, K. Yi, W. Zhang, H. Pang, S. Liu, S. Li, W. He, *Chem. Eng. J.* **2023**, *463*, 142512.
[174] Y. Duan, Y. Wang, L. Gan, J. Meng, Y. Feng, K. Wang, K. Zhou, C. Wang, X. Han, X. Zhou, *Adv. Energy Mater.* **2021**, *11*, 2004001.
[175] R. Wang, B. B. Xu, J. Wang, X. L. Wang, Y. F. Yao, *J. Mater. Chem. A* **2021**, *9*, 3985.
[176] G. Filippini, F. Longobardo, L. Forster, A. Criado, G. Di Carmine, L. Nasi, C. D'Agostino, M. Melchionna, P. Fornasiero, M. Prato, *Sci. Adv.* **2020**, *6*, 9923.
[177] Y. Xiao, Y. Leng, X. Lu, S. C. Cheng, H. Huang, M. K. Tse, J. Liang, W. Tu, C. C. Ko, X. Zhu, L. Wang, Y. Zhou, Y. Yao, Z. Zou, *J. Catal.* **2023**, *426*, 52.
[178] N. Mårtensson, J. Söderstrom, S. Svensson, O. Travnikova, M. Patanen, C. Miron, L. J. Sæthre, K. J. Borve, T. D. Thomas, J. J. Kas, F. D. Vila, J. J. Rehr, *J. Phys. Conf. Ser.* **2013**, *430*, 012131.
[179] H. Zhai, P. Tan, M. Jiang, M. Zhang, R. Ren, R. Sa, J. Pan, *ACS Catal.* **2023**, *13*, 8063.
[180] Q. Zhang, X. Chen, Z. Yang, T. Yu, L. Liu, J. Ye, *ACS Appl. Mater. Interfaces* **2022**, *14*, 3970.
[181] E. Vorobyeva, V. C. Gerken, S. Mitchell, A. Sabadell-Rendón, R. Hauert, S. Xi, A. Borgna, D. Klose, S. M. Collins, P. A. Midgley, D. M. Kepaptsoglou, Q. M. Ramasse, A. Ruiz-Ferrando, E. Fako, M. A. Ortuño, N. López, E. M. Carreira, J. Pérez-Ramírez, *ACS Catal.* **2020**, *10*, 11069.
[182] R. Qi, P. Yu, J. Zhang, W. Guo, Y. He, H. Hojo, H. Einaga, Q. Zhang, X. Liu, Z. Jiang, W. Shangguan, *Appl. Catal. B* **2020**, *274*, 119099.
[183] J. Chen, S. Fang, Q. Shen, J. Fan, Q. Li, K. Lv, *Catal.* **2022**, *12*, 962.
[184] P. Yang, L. Wang, H. Zhuzhang, R. Wang, M. M. Titirici, X. Wang, *Appl. Catal. B Environ.* **2019**, *256*, 117794.
[185] D. Zhao, J. Chen, C. L. Dong, W. Zhou, Y. C. Huang, S. S. Mao, L. Guo, S. Shen, *J. Catal.* **2017**, *352*, 491.

Manuscript received: November 28, 2023
Revised manuscript received: January 31, 2024
Accepted manuscript online: February 5, 2024
Version of record online: ■■, ■■

© 2024 The Authors. ChemCatChem published by Wiley-VCH GmbH

18673899, 0, Downloaded from https://chemistry-europe.onlinelibrary.wiley.com/doi/10.1002/cctc.202301560 by Koc University, Wiley Online Library on [12/07/2024]. See the Terms and Conditions (https://onlinelibrary.wiley.com/terms-and-conditions) on Wiley Online Library for rules of use; OA articles are governed by the applicable Creative Commons License

REVIEW



Dr. Z. Eroglu, Dr. M. S. Ozer, Prof. Ö. Metin**

1 – 25

Nitrogen-Based Imperfections in Graphitic Carbon Nitride – New Trend for Enhancing Photocatalytic Activity?

This review provides a perspective for researchers in the relevant field by depicting the challenges, providing an insightful perspective, and exploring future directions aimed at catalyzing advances in the field of N-vacancy CN for various photocatalytic applications.

18673899, 0, Downloaded from https://chemistry-europe.onlinelibrary.wiley.com/doi/10.1002/cctc.202301560 by Koc University, Wiley Online Library on [12/07/2024]. See the Terms and Conditions (https://onlinelibrary.wiley.com/terms-and-conditions) on Wiley Online Library for rules of use; OA articles are governed by the applicable Creative Commons License